New approaches to investigate the influence of orographic and dynamic blocking on large-scale atmospheric flow

Clemens Spensberger

Dissertation for the degree of Philosophiae Doctor (PhD)

Geophysical Institute
University of Bergen

October 2014

Dissertation date: 15. januar 2015

Acknowledgements

Many people contributed to the completion of this thesis, both scientifically and non-scientifically. First and foremost, I want to express my sincere gratitude to *Thomas Spengler*, for both largely giving me the freedom to pursue my own research interests while at the same time giving support and guidance whenever necessary. Although not formally supervisors, I have also strongly benefited from the interesting discussions with *Camille Li*, *Joe LaCasce* and *Sepp Egger*.

In addition, I want to thank *Michael Reeder* hosting my research visit at Monash University and the inspiring discussions during that time. Although the results of this visit did not make it into this thesis, I sincerely hope that we will have the possibility to follow up on this work at a later stage. Furthermore, I want to thank *Steve Garner* and *Isaac Held* for a very warm welcome to and instructive two weeks at GFDL. Both the visit to GFDL and the visit to Monash University were funded by *L. Meltzers Høyskolefondet* and the *Norwegian Research School in Climate Dynamics (ResClim)*.

Among my colleagues in Bergen, I want to thank *Annick* for "living with me" for almost three years and making our office such an interesting, lively and philosophical place.

This thesis would also not have been possible with out some inspiring time outside the university buildings. I therefore want to thank in particular *Aleksi*, *Steffi G.*, *Valerie*, *Kjetil*, *Selina*, *Lisbeth* and *Patrik* for the many rounds of board games, rounds of Schafkopf, quizzes, hiking and skiing trips and cosy evenings in huts. You all made my time in Bergen much more enjoyable!

Last, but definitely not least, I want to thank *Andrea* for the many visits to Bergen in particular and Norway in general. They were also a big contribution to making my time in Bergen as enjoyable as it was.

Abstract

Orographic and dynamic blocks have a profound influence on both weather and climate. The persistence of dynamic blocks can, for example, lead to the build-up of extreme temperature anomalies or droughts. In addition, previous studies linked dynamic blocks to Rossby wave breaking events, which can be associated with extreme precipitation. Dynamic blocks occur preferentially at certain locations, and therefore influence local climate. A important climatic effect of orographic blocks is to act as a temperature-barriers. For example, the North-Atlantic would be significantly colder during winter if Greenland did not shield the North-Atlantic from the climatological cold pool over the Canadian Arctic. Thus, both types of blocking contribute to the zonal asymmetries in the climate and in the atmospheric circulation.

Unfortunately, our understanding of the dynamics of both types of blocking is still far from complete. One of the main challenges in trying to grasp the essentials of blocking is the importance of non-linear effects. These effects are important, because the flow diversion around a block constitutes a large deviation from an unblocked basic state, such that the differences in the advection cannot be neglected. For that reason, previous studies proposed different indicators to capture the transition from linear flow over to non-linear flow around orography. Despite this effort, none of the proposed indicators is generally applicable. Furthermore, it is unclear how dynamic blocks interact with breaking Rossby waves and whether variability indexes like the North-Atlantic Oscillation are resulting from variability of blocking and/or wave breaking.

In this thesis, I pursue three novel approaches to enhance the understanding of blocking. First, I demonstrate that deformation is a suitable diagnostic for detecting and quantifying the magnitude of orographic and dynamic blocks. Consequently, deformation helps to investigate the splitting of synoptic systems at the Rocky-Mountain barrier. Furthermore, I show that the deformation associated with Rossby wave breaking is aligned with the observed mean deformation up and downstream of a dynamic block. Thus, the deformation associated with the wave breaking reinforces the flow diversion around the dynamic block, establishing a potential link by which Rossby wave breaking can strengthen a dynamic block.

Second, I adapt an existing scheme for upper-tropospheric jet detection. The detected jet axes open up new perspectives on the relation between jets and blocking, because they condense dynamically relevant information about the distribution of horizontal wind shear into a set of jet axis lines. Jet axes also provide the basis to directly analyse variability of the jet location. Usually, this variability is characterised indirectly by geopotential variability. I find the leading variability patterns of the jet location in the Atlantic and the Pacific to be consistent with the variability described by the North-Atlantic Oscillation and the Pacific-North American pattern, respectively. However,

in both the Atlantic and the Pacific, the second variability patterns of the jet location has no clear counterpart in the geopotential-based variability patterns. Both the East Atlantic pattern and the West Pacific pattern are related to the two leading variability patterns of the jet location.

Third, I devise and implement a new model named "Bergen dynamic model" (BEDYMO), that combines the quasi-geostrophic and dry hydrostatic primitive equations in one model. BEDYMO hence allows to easily switch between the two approximations, facilitating a direct assessment of the effect the processes that are neglected in the transition from the primitive equations to quasi-geostrophy. Therefore, BEDYMO is an ideal tool to assess the importance of these processes for simulating a given aspect of the atmospheric dynamics. Although BEDYMO is designed with an application to blocking in mind, this aspect is not limited to either type of blocking.

Contents

1 Background and Motivation

The northern hemisphere circulation features pronounced zonal asymmetries, with two distinct maxima of cyclone frequency over the Atlantic and Pacific sectors (e.g. Zishka and Smith, 1980; Wernli and Schwierz, 2006). On a hypothetical aqua planet, cyclones and anticyclones would develop and decay equally frequently at all longitudes and the circulation would be zonally symmetric. Hence, the strong asymmetries in the circulation must be induced by inhomogeneities in the lower boundary like orography or land-sea contrasts (Manabe et al., 1965; Hunt, 1973; Held and Suarez, 1994).

In order to disentangle the observed combined effect of all of the earth's inhomogeneities, it is crucial to understand how a single inhomogeneity affects the global circulation. To some extent, the effect of some types of inhomogeneities like orography or isolated heat sources can be captured by linear stationary wave theory (e.g. Smith, 1979; Hoskins and Karoly, 1981). Held (1983) even showed, that the combined atmospheric response to realistic northern hemisphere orography fits relatively well with the response in a linear model.

Nevertheless, Valdes and Hoskins (1991) and Held et al. (2002) analysed the relative importance of non-linear effects for the northern hemisphere circulation and thereby demonstrated that non-linear effects contribute significantly to the observed circulation patterns. In their analyses, one inhomogeneity sticks out in particular for its non-linear effects: the Tibetan Plateau. The plateau leads to a significant diversion of the westerlies to the north or to the south. This flow diversion is called blocking. Blocking is a non-linear effect, because it constitutes a large deviation from an unblocked basic state, such that the advection by the diverted winds is not negligible.

The diversion of the flow around the block is the characterising feature for all blocks in the atmosphere. The diversion can be around an orographic obstacle or around a body of stagnant air, where the process is called orographic or dynamic blocking, respectively. Whereas orographic blocking mainly affects the flow below crest level, dynamic blocking is generally a barotropic feature (e.g. Egger, 1978; Shutts, 1983).

Although "blocking" is a good metaphor to describe flow diversion, the term can be misleading. It implies a causality in the sense that the obstacle induces the flow diversion. While this causality is clear for orographic blocking, the relation between the diverted flow and the block is not as straightforward for dynamic blocking. It is a matter of ongoing debate if the body of stagnant air in a dynamic block is causing the flow diversion or if it is a result of the flow diversion (Colucci, 1985; Nakamura and Wallace, 1993; Swanson, 2001). As with most chicken-and-egg conundrums, there is likely no clear-cut solution to this ambiguity.

Orographic blocking can have a significant impact on the synoptic development.

For example, cyclones forming along the North American east coast often interact with Greenland in their developing stage. Depending on the exact location of the cyclone, this interaction can lead to tip jets at the southern tip of Greenland or to barrier jets along the east coast of Greenland (e.g. Doyle and Shapiro, 1999; Moore and Renfrew, 2005; Harden et al., 2011). Våge et al. (2009) showed that these high-wind events also strongly influence mixed layer depth in the seas around Greenland.

Dynamical blocking is often linked to extreme events. Some of these extremes are caused by the stationarity of the weather situation. Persistent local imbalances in, for example, the energy budget can lead to a build-up of extreme temperature anomalies. In regions that receive anomalously little precipitation during a block, the block can additionally lead to droughts. Both the Russian heat wave in 2010 and the quasi-stationary block over the Eastern Pacific during winter 2013/14 are examples for such events (Dole et al., 2011; Wallace et al., 2014). In both examples, the stationarity of the block caused record-breaking temperatures.

Another more indirect link between blocking and extreme events is through breaking Rossby waves (McIntyre and Palmer, 1983; Thorncroft et al., 1993; Appenzeller et al., 1996). When a Rossby wave breaks, its wavelength is gradually shortened until the wave collapses into an thin filament. There is growing evidence for close relation between dynamic blocking and Rossby wave breaking, although the underlying mechanism is still poorly understood (Benedict et al., 2004; Altenhoff et al., 2008; Woollings et al., 2008). Altenhoff et al. (2008) for example showed, that there are preferred locations of Rossby wave breaking directly up- and downstream of a block, but did not propose a potential mechanism explaining this finding.

Rossby wave breaking events are often linked to extreme weather, because they go along with transport in the upper troposphere of either subtropical air far to the north or polar air far to the south. Southward protrusions of polar air masses at upper levels destabilise the air column and can lead to extreme convective precipitation. Massacand et al. (1998) showed that several extreme precipitation events in the Alpine region were associated with Rossby wave breaking events.

Because of those connections to extreme weather events, the ability to reliably forecast dynamic blocking episodes has great societal value. Unfortunately, forecasting the onset and decay of such episodes remains a challenge (Tibaldi and Molteni, 1990; Pelly and Hoskins, 2003b; Matsueda et al., 2011; Jia et al., 2014). A potential reason why these aspects are relatively poorly forecasted might be the importance of non-linear processes, which can quickly amplify initially small forecast errors and biases (Lorenz, 1963; Benzi et al., 1986).

In addition to shaping day-to-day weather, blocking also has a profound influence on the mean climate. Both orographic and dynamic blocking occur preferentially in specific regions, thereby playing an important role in shaping the regional climate. For example, one important climatic effect of blocking orography can be to act as a temperature barrier. The barrier effect has been shown to be important for the North Atlantic climate, where Greenland shields the area from the climatological cold pool located over the Canadian Arctic (Petersen et al., 2004; Junge et al., 2005). Furthermore, Boos and Kuang (2010) showed that it is the barrier effect of the Himalayas that is pivotal for the dynamics of the Indian monsoon, rather than the climatological low over the

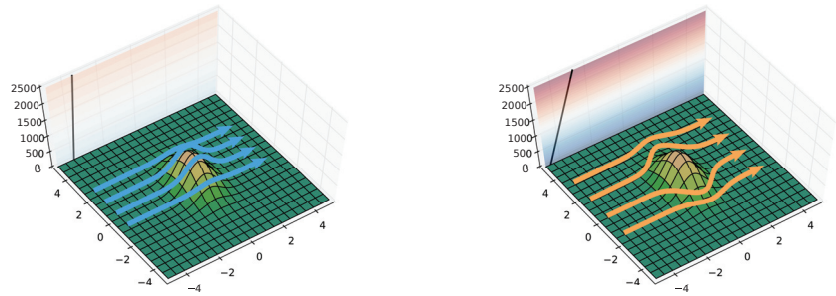

Figure 1: Linear and and blocked flow past an isolated Gaussian mountain. In the blocked case, the approaching flow is diverted around the orography in the *xy*-plane.

Tibetan Plateau. Here, the Himalayas constitute a barrier between the hot and humid Indian peninsula and the cold and dry Inner Asia.

Given these implications, it is not surprising that both types of blocking have been intensively studied before. Despite all the effort, however, the overall understanding of blocking is far from complete. In the following sections, I summarise pertinent earlier results, that directly lead to the open questions that I will address in this thesis.

1.1 Orographic blocking

One of the obstacles to better understand blocking are the already mentioned challenges posed by the importance of non-linear processes. While linear models of flow–orography interaction can explain, for example, the excitation of Rossby and gravity waves (e.g. Smith, 1979; Hoskins and Karoly, 1981), blocking is excluded from these models, because blocking is a non-linear process. Figure 1 illustrates the flow diversion around a mountain and contrasts that flow regime with linear flow over the mountain.

Probing the limits of the applicability of linear theory, many studies investigated the transition from a linear to a non-linear regime and tried to grasp its essence in characteristic numbers. One widely accepted number designed for this purpose is the so-called mountain Froude number

$$Fr_m = \hat{h}_m^{-1} := \frac{U}{N h_m} \quad , \tag{1}$$

with U being a characteristic wind speed, N a characteristic Brunt-Väisälä frequency and h_m the height of the mountain (e.g. Sheppard, 1956; Snyder et al., 1985; Smith, 1989). Some authors prefer the inverse of the mountain Froude number and denote it non-dimensional mountain height $\hat{h}_m$. It arises as a common coefficient for non-linear terms in the non-dimensionalised incompressible primitive equations (Smith and Grønås, 1993).

From numerous numerical model experiments it has however become clear, that the mountain Froude number does not capture all factors influencing the transition from

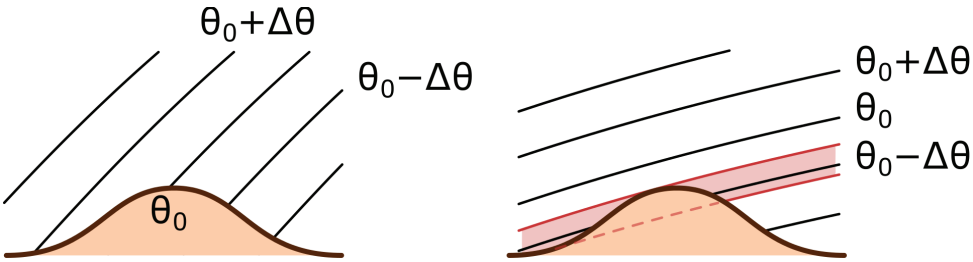

Figure 2: Vertical cross-sections with unblocked and blocked isentropes past an isolated mountain. In the blocked case, the some isentropes intersect more than once with the lower surface, as indicated by the red layer, showing that the mountain protrudes these surfaces.

the linear to the non-linear regime. Other factors are the meridional scale of the mountain, its latitude, and the vertical wind shear, among others (Trenberth and Chen, 1988; Smith and Grønås, 1993; Ringler and Cook, 1995; Thorsteinsson and Sigurdsson, 1996; Ringler and Cook, 1997; Petersen et al., 2003). Hence, the mountain Froude number can only give a rough indication on the importance of non-linear effects.

A further obstacle to the application of the Froude number to real synoptic situations is the use of characteristic scales for the wind speed, and the stratification. The determination of these scales is ambiguous in real situations. Consequently, one has to rely on spatial and/or temporal averaging to define the ingredients of Fr_m. As the flow in the vicinity of mountains tends to be particularly inhomogeneous, this averaging will always lead to a certain degree of arbitrariness in the evaluation of Fr_m. Even for a very idealised mountain, Reinecke and Durran (2008) could not identify a single best method to determine the Brunt-Väisälä frequency under varying atmospheric conditions, thereby questioning the representativeness of the spatially averaged Fr_m for the local dynamics.

Schär and Davies (1988), Valdes and Hoskins (1991), and Cook and Held (1992) proposed a different criterion to unify all these influencing factors into one compact indicator. They assume adiabatic motions, such that the flow cannot leave its isentropic surface. Hence, the flow must be diverted around any mountain that protrudes this isentropic surface. As analogous arguments apply for fluid parcels on any isentropic surface, some surfaces will be blocked as soon as the meridional slope of a mountain is steeper than the slope of the isentropic surfaces close to the orography (Fig. 2). This criterion can be expressed as (adapted from Cook and Held, 1992)

$$\left| l_y \frac{\partial \theta_0}{\partial y} \right| < h_m \frac{\partial \theta_0}{\partial z} \quad , \tag{2}$$

using some of the above scales and with l_y the meridional length scale of the mountain and θ_0 the basic-state potential temperature. For an application to real synoptic situations, the criterion can be generalised to test for the existence of protrusions of orography through the instantaneous isentropic surfaces. Any such protrusion constitutes a block, because adiabatic flow is diverted around the orography.

Although this isentropic criterion provides a perspicuous criterion for analysing idealised model simulations, its application to real weather situations is not straight-

forward. Close to the sea or land surfaces, where radiation imbalances and boundary layer transports play an important role, the underlying assumption of adiabatic motion is rather unrealistic.

Furthermore, the criterion becomes conceptually misleading, if there is a pronounced temperature contrast between the upstream and the downstream side of the mountain, rendering the orography a temperature barrier. Such a temperature contrast often exists for Greenland in winter, with the cold ice-covered Labrador to the West and the comparably warm Atlantic to the East. In this case, isentropic surfaces that exist on the cold side of the mountain would be well below the surface on the warm side. Consequently, the flow is not diverted around the mountain, but must remain upstream of the mountain. From an isentropic perspective this blocked situation is indistinguishable from an intersection of an isentropic surface with a flat land surface where the flow would not be considered as orographically blocked.

Some insight in the non-linear dynamics of blocking is provided by studies on lee cyclogenesis and on the interaction of cold fronts with orography (Davies, 1984; Egger and Hoinka, 1992; Egger, 1995). These studies consider two-dimensional flow in two or three homogeneous layers approaching a razor-thin barrier or a finite-width ridge. The biggest limitation of these models is the two-dimensionality, which does not permit a flow-diversion around the orography, but requires blocked flow to stagnate upstream. For this reason, these models are only applicable to orographic barriers like the Rocky Mountains which extend far enough meridionally that flow around the orography is not easily possible.

Despite the mentioned shortcomings of these concepts, the Froude number, the isentropic-protrusion concept, and the two-dimensional cold-air damming model provide a context to interpret the results from the numerous studies investigating orographic blocks using numerical models (e.g. Smolarkiewicz and Rotunno, 1989; Yu and Hartmann, 1995; Doyle and Shapiro, 1999; Petersen et al., 2003), case studies (e.g McCauley and Sturman, 1999; Outten et al., 2009) and observations (e.g. Parish, 1982; Mc Innes et al., 2009). The variety of features documented in these studies highlights the complexity of flow–orography interactions, but did not lead to more generally applicable concepts, neither for the description of the transition between the linear and the non-linear regimes nor for the description of the non-linear dynamics.

1.2 Dynamic blocking

Whereas flow diversion around an orographic obstacle unambiguously indicates orographic blocking, flow diversion around an anticyclone does not necessarily imply a dynamic block. The exact criteria to separate blocking anticyclones from non-blocking anticyclones are not obvious and still a matter of debate. In one of the first attempts to define objective criteria for mid-latitude blocks, Rex (1950) required

1. a splitting of the westerly flow into two relatively equal branches,
2. an abrupt transition from a zonal flow into meridional flow at the location of the flow splitting,

3. a minimum zonal extent and

4. a minimum duration.

To be able to objectively detect blocking in one of the first gridded reanalysis datasets, Lejenäs and Økland (1983) successfully combined requirement (1)–(3) by looking for geopotential gradient reversals between two fixed latitudes spanning the mid-latitude westerlies. The approach was refined in many later studies by allowing for variations in the blocked range of latitudes and avoiding some classes of spurious detections by additional criteria (e.g. Tibaldi and Molteni, 1990; Barriopedro et al., 2006). Pelly and Hoskins (2003a) adapted the approach to the potential vorticity (PV) perspective by considering reversals of potential temperature gradients on PV surfaces.

The evolution of the criteria for dynamic blocking followed the changing dynamical interpretation of blocks. For example, the second requirement of Rex (1950) is heavily influenced by his interpretation of dynamic blocking as a process analogous to a hydraulic jump. Analogous to an hydraulic jump, he imagines dynamic blocking to be associated with a change in flow regime from "supercritical" focused strong westerly flow to a "subcritical" broad flow of weak westerlies. Although this conceptual model was later discarded by Egger (1978), Rex (1950) already noticed a relation of blocking with "intense cyclonic vortices" upstream of the block, which also play an integral role in much more recent conceptual ideas about blocking (e.g. Altenhoff et al., 2008).

Many authors have proposed alternative mechanisms for blocking. Arakawa (1952) noticed that some essential aspects of blocking can already be captured by linear analytical wave theory, whereas Namias (1964),White and Clark (1975), and Kalnay-Rivas and Merkine (1981) point out that the observed preferred locations of blocking can be related to stationary forcing like orography. Egger (1978) successfully combined these two perspectives in barotropic and baroclinic numerical models, and concludes that blocking results from non-linear interactions between slowly-moving waves and stationary forcing.

Later, Shutts (1983) and Haines and Marshall (1987) showed that blocking can also arise purely by non-linear interactions of synoptic-scale eddies. This process can however not explain the zonal asymmetries in the blocking location. Therefore, Luo (2005) augmented the eddy-interactions framework with stationary forcing like orography. Swanson (2000) and Swanson (2001) pursued a related, but different approach. He interpreted blocking onset as an instability of a boundary separating two homogeneous PV reservoirs. The studies of Shutts (1983), Haines and Marshall (1987), Swanson (2001), and Luo (2005) all require non-linear eddy interactions and hence provide the foundation for studies arguing for a close dynamical relation between dynamic blocking and Rossby wave breaking.

The potential relation between blocking and wave breaking is already apparent from the overlapping definitions of Rossby wave breaking and blocking. Rossby wave breaking is the overturning of PV contours on isentropic surfaces (McIntyre and Palmer, 1983; Thorncroft et al., 1993; Appenzeller et al., 1996) leading to a reversed PV gradient. Pelly and Hoskins (2003a), Schwierz et al. (2004), and Berrisford et al. (2007) use this reversed gradient to detect dynamic blocking events. Consistently, Altenhoff et al. (2008) find a climatological co-occurrence of blocking and wave breaking, and

demonstrate that there is a preferred location for cyclonic (anticyclonic) wave breaking just upstream (downstream) of the block.

The interplay between blocking and wave breaking might also be largely responsible for the variability captured by indexes such as the North-Atlantic Oscillation (NAO) or the Pacific-North American (PNA) pattern. Renwick and Wallace (1996) and Croci-Maspoli et al. (2007) documented an increased frequency of blocking occurrence during positive phases of the PNA and the NAO, respectively. However, in a stream function budget analysis, Feldstein (2002), and Feldstein (2003) found the life cycle of the PNA to be dominated by linear processes, whereas nonlinear processes dominate for the NAO. These fundamental differences in the stream function budget contradict Croci-Maspoli et al. (2007), who imply that the same mechanism is active in both the Atlantic and the Pacific. Furthermore, Benedict et al. (2004) and Woollings et al. (2008) proposed different interpretations of the NAO, but both argue for a close dynamical relation between wave breaking events, blocking, and the NAO.

The NAO and the PNA indexes are commonly based on Empirical Orthogonal Functions (EOF) of the geopotential and hence directly incorporate the variability created by the geopotential anomaly associated with a block (e.g. Wallace and Gutzler, 1981; Barnston and Livezey, 1987). If these variability indexes are indeed driven by blocking or wave breaking, jet and storm track diagnostics should display variability patterns that are consistent with the geopotential-based EOFs. However, Athanasiadis et al. (2010) and Wettstein and Wallace (2010) demonstrated that not all of these indexes relate to leading variability patterns of the zonal wind and different storm track diagnostics, respectively. Although they do not discuss the implications of their results for the offered dynamical relations between the NAO, PNA, and blocking, their results show that these relations are far from being fully understood.

1.3 Open questions, remaining challenges

Despite all the efforts to better understand both types of blocking, there are still many questions that are not resolved satisfactorily. For orographic blocking, there is no generally applicable diagnostic indicating the transition from the linear to the non-linear flow regime that would allow to define the limits of linear theories. Furthermore, there is little conceptual consensus on how to best describe non-linear flow–orography interactions.

For dynamic blocking, there seems to be an emerging consensus on the objective criteria defining a block. In addition, the conceptual frameworks combining stationary forcing with either slowly-moving linear waves (Egger, 1978) or non-linear eddy interactions (Luo, 2005) can explain many features of blocking. However, some questions like the dynamic link to Rossby wave breaking or to common variability indexes remain rather poorly understood (e.g. Feldstein, 2002; Croci-Maspoli et al., 2007).

In summary, some particular open questions regarding both types of blocking are:

1. How can we reliably detect orographic and dynamic blocking and quantify the intensity of the block?

2. Which processes determine the occurrence of blocking and the transition between a blocked and unblocked state?

3. What is the simplest model representing the processes that determine the dynamics of blocking?

In addition, previous studies on dynamic blocking raised the questions:

4. Is there a dynamical link between blocking and Rossby wave breaking? If yes, which processes constitute this link?

5. Do variability indexes like the NAO and the PNA describe variability in the occurrence of blocking?

The main aim of this thesis is to establish and apply new approaches that help answering these questions.

2 The novel approaches in this thesis

The introduction posed five questions regarding the influence of orographic and dynamic blocking on large-scale atmospheric flow. To be able address these questions, I devised three new approaches that help to study interactions between orography, blocking, and jet streams. They are:

1. **The use of deformation as a diagnostic for both types of blocking.**

   Deformation is a promising diagnostic to detect orographic and dynamic blocking (question 1), because the flow diversion around an obstacle elongates approaching fluid parcels around the block. The elongation is reflected in a characteristic deformation pattern. In contrast to the Froude number, deformation avoids the use of characteristic scales that are not uniquely determined in real cases. Like vorticity and divergence, deformation instead describes the local properties of a flow field. Therefore, deformation provides local information on the intensity of the block and does not require any averaging.

   Furthermore, Rossby waves are severely deformed during the wave breaking process. Hence, this process must be associated with a clear signature in the deformation field. The role of deformation in both wave breaking and blocking opens up an avenue to investigate potential dynamical links between these processes (questions 2 & 4).

   This approach is described and applied in Paper I and II. A brief discussion of the physical mechanisms creating and destroying deformation is given in Appendix A.

2. **The use of jet axes as diagnostic condensing information on internal structure of jets and for describing the variability of the jet location.**

   Jets are often detected by applying a wind speed threshold to define the perimeter and hence the body of a jet stream (e.g. Koch et al., 2006; Strong and Davis, 2007; Woollings et al., 2010). A disadvantage of this approach is that it tends to conceal the existence of multiple wind speed maxima within one jet body. These wind maxima, however, define the structure of the wind shear within a jet body, which separates the areas dominated by cyclonic or anticyclonic wave breaking (Rivière, 2009; Barnes and Hartmann, 2012). Hence, the locations of these wind speed maxima are of great dynamical interest. As jets are elongated, these wind speed maxima generally follow a line, called the jet axis. In addition to being related to the wind shear distribution, this axis also characterises the exact location of a jet.

   Furthermore, jet axes allow to independently detect dynamic blocking episodes by the associated splitting of the jet into two branches (question 1). Hence, the

distribution of jet axes for different phases of common variability indexes can give independent indications for or against the proposed interpretations of these indexes as being essentially driven by blocking (question 5).

This approach is described and applied in case studies in Paper III and applied to jet variability in Paper IV.

3. **The introduction of a new idealised atmospheric model that incorporates a hierarchy of approximations to the primitive equations in one consistent framework.**

   In order to investigate specific processes one should ideally be able to switch between levels of complexity in a hierarchy of approximations. As most atmospheric models are based on one approximation, one would hence need to compare different models. These models can differ regarding the numerics, the implementation of boundary conditions, and the model configuration, among other features. These differences in the model formulation introduce non-physical differences in the model results that complicate the comparison. By combining quasi-geostrophy and the the dry hydrostatic primitive equations into one framework, we can eliminate most of these non-physical differences. The combined model is then an ideal test bed to isolate the fundamental aspects of the dynamics underlying orographic and dynamical blocking by testing which of the neglected or included terms are essential to simulate either type of blocking (question 2 & 3).

   This approach and the model is documented in Paper V, and the full derivation of the model equations is given in Appendix B.

3 Summary of the results

Whereas Papers I, III and V are mainly—but not entirely—concerned with the establishment and the implementation of the three novel approaches, Papers II and IV showcase some immediate applications of the approaches to address the questions raised in section 1.3. In the following, I summarise the main findings for each Paper.

- **Paper I: A new look at deformation as a diagnostic for large-scale flow**
  Spensberger, C. and Spengler, T. (2014), *Journal of Atmospheric Sciences*, 71, 4221–4234.

  In this paper, we demonstrate that deformation captures local information on the strength of the flow diversion around an orographic or dynamic block. For that reason, we conclude that deformation is suitable to detect blocking and to quantify the intensity of the block (question 1).

  Furthermore, we show that Rossby wave breaking is associated with a characteristic structure in the deformation field. The orientation of the deformation is such that cyclonic (anticyclonic) wave breaking upstream (downstream) of a block enhances the flow diversion around the block (questions 2 & 4). This is exactly the preferred region of wave breaking that Altenhoff et al. (2008) find in their climatology. Hence, the typical configuration of blocks and wave breaking is such that wave breaking enhances the flow diversion around the block. Therefore, we conclude that deformation indeed provides a dynamical link between blocking and wave breaking that can potentially explain how Rossby wave breaking events create and maintain a block.

- **Paper II: The splitting of synoptic systems at the Rocky Mountains barrier**
  Egger, J., Spensberger, C. and Spengler, T. (2014), in preparation for *Monthly Weather Review*.

  In this paper, we analyse the composite evolution of the 1 % strongest synoptic systems approaching and crossing the Rocky Mountains. While the lower part of an approaching cyclonic or anticyclonic anomaly is blocked by the mountain range, the upper-level anomaly propagates comparatively undisturbed across the barrier. For cyclonic systems, the lower part is blocked, resulting in a splitting of the system. Furthermore, cyclogenesis occurs in the lee. Following up on the ideas of Paper I, we also use deformation to discuss the dynamical evolution of and the differences between the cyclonic and the anticyclonic composites.

  The synoptic evolution in the two cases allows us to conclude, which of the published theories for cyclone–orography interactions appropriately describe the effect of the Rocky Mountains on strong synoptic systems (question 2). In particu-

lar, the comparison between the cyclonic and the anticyclonic composites facilitates an assessment of the limits of linear theories describing this interaction. Although, we limit our analysis to the 1 % strongest synoptic systems, some features like the deflection of the blocked lower part of the systems towards the north appears analogous for the cyclonic and the anticyclonic case. However, the synoptic development in the lee of the Rocky Mountains differs considerably between the cyclonic and the anticyclonic cases.

- **Paper III: Upper tropospheric jet axis detection and application to the boreal winter 2013/14**
  Spensberger, C., Spengler, T., and Li, C. (2014), in preparation for *Monthly Weather Review*.

  In this paper, we adapt the jet axis detection scheme devised by Berry et al. (2007) for detecting African Easterly Jets to be suitable for upper tropospheric jet detection. We demonstrate the advantages of our scheme over previous jet identification methods by comparing the different methods for synoptic situations during the boreal winter 2013/14 as well as for the climatology for 1979–2013. The winter 2013/14 featured a long-lasting blocking episode in the East Pacific. We discuss potential dynamical implications of the detected jet axes by relating them to the conceptual model of Dritschel and McIntyre (2008), who analysed the effect of growing baroclinic eddies on the jet axis (questions 1 & 4).

  In addition, we show that the jet axis detection scheme also works reliably for time-averaged input data. Although the use of monthly wind averages as basis for the jet axis detection drastically reduces the variability of the jet axis location, it does not introduce any spatial biases in the location.

- **Paper IV: Wintertime variability of mid-latitude jet axes**
  Spensberger, C., Spengler, T., and Li, C. (2014), in preparation for *Journal of Climate*.

  In this study, we investigate the variability of jet axes detected by the scheme introduced in Paper III. Through EOF analysis, we identify variability patterns of the Atlantic and Pacific jet axis location. Over both ocean basins the two leading variability patterns of the jet axis are a tripole pattern reflecting the transition between a straight and an undulating jet stream, as well as a dipole pattern reflecting meridional shifts of the jet location. We denote the tripole as a "straightening" pattern. These variability patterns are consistent with the variability patterns of Athanasiadis et al. (2010) and Wettstein and Wallace (2010), who analysed variability of the zonal wind, and several storm track diagnostics, respectively.

  Composites of the jet axis distribution for positive and negative phases of the NAO describe shifts in the latitude of the eddy-driven jet that co-occur with a straightening of the subtropical jet over the Atlantic and the African continent. The PNA describes a variation in the length of the Pacific jet that extends either to the North American west coast or the date line. Both the West-Pacific (WP) pattern and the East-Atlantic (EA) pattern do not have a clear-cut effect on the jet axis distribution. In addition, both the WP and the EA correlate to both of our

leading EOFs in the respective ocean basin. Hence, they constitute a mixture of different variability patterns of the jet location.

- **Paper V: Bedymo, a combined quasi-geostrophic and primitive equations model**
  Spensberger, C., Thorsteinsson, T., Spengler, T. (2014), in preparation for *Geoscientific Model Development*.

  The use of the two-column layout of the journal Geoscientific Model Development shall not indicate, that this manuscript already went through the discussion process for this journal. I use this layout, because the layout for Geoscientific Model Development Discussions is unfortunately not suitable be to included in this thesis.

  In this paper, we introduce the BErgen DYnamic MOdel (BEDYMO), which employs a common approach to solve the quasi-geostrophic (Charney, 1947) and hydrostatic primitive equations. BEDYMO aims to keep the time-integration procedure as similar as possible for the two approximations (detailed derivation in Appendix B). The similarity allows us to easily and consistently switch between the approximations by neglecting or considering the respective terms in the equations. To demonstrate the performance BEDYMO, we evaluate the model against the analytical solutions or conceptual models for (a) cyclogenesis in a baroclinically unstable environment, (b) stationary Rossby waves excited by orography, and (c) the coupled response to an equatorial temperature anomaly in the ocean mixed layer. For the coupled test, we use a slab-ocean with different parametrisations of the oceanic heat transport. For all three test cases, BEDYMO compares well to the analytic solution or the conceptual models. Furthermore, these test cases highlight the dynamical differences arising from the different approximations, demonstrating that the model is suitable to address question 3.

Naturally, the results of these five papers do not fully answer all five questions raised in section 1.3. Nevertheless, they contribute to the understanding of orographic and dynamic blocking and thereby demonstrate the value of the new approaches established in this thesis.

I am convinced that these approaches will prove to be instructive also outside the theme of blocking. Some potential continuations of this work and other applications of the approaches are described in the following.

4 Outlook

A large part of this thesis is devoted to the description of new approaches to study orographic and dynamic blocking. Every approach by itself opens up new perspectives on these phenomena and provides the basis for the conclusions drawn in this thesis. However, a combined analysis using several of these approaches might prove to be even more insightful.

The following sections outline potential future paths of research building on the results in this thesis. The first pair of suggestions are more direct continuations of this thesis, as they also focus on blocking. The third suggestion demonstrates that the new approaches are equally valuable outside the direct scope of this thesis.

4.1 Dynamics of orographic blocking

The combination of Paper I and Paper V facilitates the identification the minimal model required to represent pertinent aspects of orographic blocking. Paper I documents the deformation patterns associated with orographic blocking, both in reanalysis data and analytically for two-dimensional flow around a circular obstacle. These results provide a base line to compare with the simulated flow diversion around idealised and realistic topography in the different approximations available in BEDYMO . The similarity between the base line and simulated deformation patterns can serve as a benchmark of how well blocking is simulated. This allows to identify the minimal model.

The minimal model can subsequently be used to clarify which of the proposed parameters are best suited to indicate the transition between linear and non-linear flow (see discussion and references in sec. 1.2). By analysing the sensitivity of the simulated orographic blocking response to variations of each parameter, BEDYMO allows us to identify those parameters that are best suited as an indicator for this transition.

4.2 Dynamics of dynamic blocking and its relation to jet variability

Combining Papers I and III-V in this thesis, a similar strategy will help to better understand dynamic blocking and jet variability. Long-term simulations of a baroclinic channel including thermal driving allow us to directly relate the jet driving mechanisms to the simulated jet variability (Paper III-IV; Eichelberger and Hartmann, 2007; Li and Wettstein, 2012). Furthermore, the deformation patterns described in Paper I allow us to analyse blocking variability. The sensitivity of these variability patterns can then be

tested by varying the relative importance of the driving mechanisms within the different approximations available in BEDYMO. This set of simulations can help to further clarify the physical mechanisms relating the driving mechanisms to jet and blocking variability.

4.3 Interaction of fronts with orography

This thesis was only concerned with flow at the synoptic and larger scales. The same approaches will, however, be equally valuable at smaller scales, for example to study the interaction of fronts with orography. Published theories on this interaction (e.g. Davies, 1984; Blumen and Gross, 1987) fail to explain the complex structures that are documented for numerous case studies (Egger and Hoinka, 1992; Blumen, 1992; Schär, 2002; Neiman et al., 2004).

Similar to orographic blocking, one of the fundamental questions regarding this interaction is whether the flow moves over the mountain or around it. The large spatial variability of the flow around the steep and complex orography that is resolved on smaller scales will render the Froude number even less suitable for identifying the flow regime. Also two-dimensional deformation, as discussed in Paper I, becomes inappropriate on these scales, because vertical velocities become important. The concept can, however, be extended to three-dimensional flow and give local information on the flow diversion on smaller scales analogously to Paper I. This local information can provide a basis to define different categories of front interactions and hence helps to conceptually divide between classes of such interactions. By simulating archetypal interactions for each class, BEDYMO can point to the dominant dynamical processes for each class separately and thus help to understand the dynamical differences.

Bibliography

Altenhoff, A. M., Martius, O., Croci-Maspoli, M., Schwierz, C., and Davies, H. C.: Linkage of atmospheric blocks and synoptic-scale Rossby waves: a climatological analysis, Tellus A, 60, 1053–1063, doi:10.1111/j.1600-0870.2008.00354.x, URL http://dx.doi.org/10.1111/j.1600-0870.2008.00354.x, 2008.

Appenzeller, C., Davies, H. C., and Norton, W. A.: Fragmentation of stratospheric intrusions, Journal of Geophysical Research: Atmospheres, 101, 1435–1456, doi:10.1029/95JD02674, URL http://dx.doi.org/10.1029/95JD02674, 1996.

Arakawa, H.: Kinematics of Meandering and Blocking Actionof the Westerlies:, Papers in Meteorology and Geophysics, 3, 12–18, 1952.

Athanasiadis, P. J., Wallace, J. M., and Wettstein, J. J.: Patterns of Wintertime Jet Stream Variability and Their Relation to the Storm Tracks*, J. Atmos. Sci., 67, 1361–1381, URL http://dx.doi.org/10.1175/2009JAS3270.1, 2010.

Barnes, E. A. and Hartmann, D. L.: Detection of Rossby wave breaking and its response to shifts of the midlatitude jet with climate change, Journal of Geophysical Research: Atmospheres, 117, n/a–n/a, doi:10.1029/2012JD017469, URL http://dx.doi.org/10.1029/2012JD017469, 2012.

Barnston, A. G. and Livezey, R. E.: Classification, Seasonality and Persistence of Low-Frequency Atmospheric Circulation Patterns, Mon. Wea. Rev., 115, 1083–1126, URL http://dx.doi.org/10.1175/1520-0493(1987)115<1083:CSAPOL>2.0.CO;2, 1987.

Barriopedro, D., García-Herrera, R., Lupo, A. R., and Hernández, E.: A Climatology of Northern Hemisphere Blocking, J. Climate, 19, 1042–1063, URL http://dx.doi.org/10.1175/JCLI3678.1, 2006.

Benedict, J. J., Lee, S., and Feldstein, S. B.: Synoptic View of the North Atlantic Oscillation, J. Atmos. Sci., 61, 121–144, URL http://dx.doi.org/10.1175/1520-0469(2004)061<0121:SVOTNA>2.0.CO;2, 2004.

Benzi, R., Malguzzi, P., Speranza, A., and Sutera, A.: The statistical properties of general atmospheric circulation: Observational evidence and a minimal theory of bimodality, Quarterly Journal of the Royal Meteorological Society, 112, 661–674, doi:10.1002/qj.49711247306, URL http://dx.doi.org/10.1002/qj.49711247306, 1986.

Berrisford, P., Hoskins, B. J., and Tyrlis, E.: Blocking and Rossby Wave Breaking on the Dynamical Tropopause in the Southern Hemisphere, J. Atmos. Sci., 64, 2881–2898, URL http://dx.doi.org/10.1175/JAS3984.1, 2007.

Berry, G., Thorncroft, C., and Hewson, T.: African Easterly Waves during 2004–Analysis Using Objective Techniques, Mon. Wea. Rev., 135, 1251–1267, doi:10.1175/MWR3343.1, URL http://dx.doi.org/10.1175/MWR3343.1, 2007.

Blumen, W.: Propagation of fronts and frontogenesis versus frontolysis over orography, 48, 37–50–, URL http://dx.doi.org/10.1007/BF01029558, 1992.

Blumen, W. and Gross, B. D.: Advection of a Passive Scalar over a Finite-Amplitude Ridge in a Stratified Rotating Atmosphere, J. Atmos. Sci., 44, 1696–1705, URL http://dx.doi.org/10.1175/1520-0469(1987)044<1696:AOAPSO>2.0.CO;2, 1987.

Boos, W. R. and Kuang, Z.: Dominant control of the South Asian monsoon by orographic insulation versus plateau heating, Nature, 463, 218–222, doi:doi:10.1038/nature08707, 2010.

Charney, J. G.: The dynamics of long waves in a baroclinic westerly current, J. Meteorol., 4, 135–163, URL http://ci.nii.ac.jp/naid/10019920229/en/, 1947.

Colucci, S. J.: Explosive Cyclogenesis and Large-Scale Circulation Changes: Implications for Atmospheric Blocking, J. Atmos. Sci., 42, 2701–2717, doi:10.1175/1520-0469(1985)042<2701:ECALSC>2.0.CO;2, URL http://dx.doi.org/10.1175/1520-0469(1985)042<2701:ECALSC>2.0.CO;2, 1985.

Cook, K. H. and Held, I. M.: The Stationary Response to Large-Scale Orography in a General Circulation Model and a Linear Model, Journal of the Atmospheric Sciences, 49, 525–539, doi:10.1175/1520-0469(1992)049<0525:TSRTLS>2.0.CO;2, URL http://journals.ametsoc.org/doi/abs/10.1175/1520-0469%281992%29049%3C0525%3ATSRTLS%3E2.0.CO%3B2, 1992.

Croci-Maspoli, M., Schwierz, C., and Davies, H.: Atmospheric blocking: space-time links to the NAO and PNA, Climate Dynamics, 29, 713–725, doi:10.1007/s00382-007-0259-4, URL http://dx.doi.org/10.1007/s00382-007-0259-4, 2007.

Davies, H.: On the orographic retardation of a cold front, Beiträge zur Physik der Atmosphäre, 57, 409–418, 1984.

Dole, R., Hoerling, M., Perlwitz, J., Eischeid, J., Pegion, P., Zhang, T., Quan, X.-W., Xu, T., and Murray, D.: Was there a basis for anticipating the 2010 Russian heat wave?, Geophys. Res. Lett., 38, L06 702–, URL http://dx.doi.org/10.1029/2010GL046582, 2011.

Doyle, J. D. and Shapiro, M. A.: Flow response to large-scale topography:the Greenland tip jet, Tellus A, 51, 728–748, doi:10.1034/j.1600-0870.1996.00014.x, URL http://dx.doi.org/10.1034/j.1600-0870.1996.00014.x, 1999.

Dritschel, D. G. and McIntyre, M. E.: Multiple Jets as PV Staircases: The Phillips Effect and the Resilience of Eddy-Transport Barriers, J. Atmos. Sci., 65, 855–874, doi:10.1175/2007JAS2227.1, URL http://dx.doi.org/10.1175/2007JAS2227.1, 2008.

Egger, J.: Dynamics of Blocking Highs, J. Atmos. Sci., 35, 1788–1801, doi:10.1175/1520-0469(1978)035<1788:DOBH>2.0.CO;2, URL http://dx.doi.org/10.1175/1520-0469(1978)035<1788:DOBH>2.0.CO;2, 1978.

Egger, J.: Interaction of cold-air blocking and upper-level potential vorticity anomalies during lee cyclogenesis, Tellus A, 47, 597–604, doi:10.1034/j.1600-0870.1995.00107.x, URL http://dx.doi.org/10.1034/j.1600-0870.1995.00107.x, 1995.

Egger, J. and Hoinka, K.: Fronts and orography, Meteorol. Atmos. Phys., 48, 3–36–, URL http://dx.doi.org/10.1007/BF01029557, 1992.

Egger, J., Spensberger, C., and Spengler, T.: The splitting of synoptic systems at the Rocky Mountains barrier, J. Atmos. Sci., in preparation, 2014.

Eichelberger, S. J. and Hartmann, D. L.: Zonal Jet Structure and the Leading Mode of Variability, J. Climate, 20, 5149–5163, URL http://dx.doi.org/10.1175/JCLI4279.1, 2007.

Feldstein, S. B.: Fundamental mechanisms of the growth and decay of the PNA teleconnection pattern, Quarterly Journal of the Royal Meteorological Society, 128, 775–796, doi:10.1256/0035900021643683, URL http://dx.doi.org/10.1256/0035900021643683, 2002.

Feldstein, S. B.: The dynamics of NAO teleconnection pattern growth and decay, Quarterly Journal of the Royal Meteorological Society, 129, 901–924, doi:10.1256/qj.02.76, URL http://dx.doi.org/10.1256/qj.02.76, 2003.

Haines, K. and Marshall, J.: Eddy-Forced Coherent Structures As A Prototype of Atmospheric Blocking, Quarterly Journal of the Royal Meteorological Society, 113, 681–704, doi:10.1002/qj.49711347613, URL http://dx.doi.org/10.1002/qj.49711347613, 1987.

Harden, B. E., Renfrew, I. A., and Petersen, G. N.: A Climatology of Wintertime Barrier Winds off Southeast Greenland, J. Climate, 24, 4701–4717, doi:10.1175/2011JCLI4113.1, URL http://dx.doi.org/10.1175/2011JCLI4113.1, 2011.

Held, I. M.: Stationary and quasi-stationary eddies in the extratropical troposphere: Theory, Large-scale dynamical processes in the atmosphere, pp. 127–168, 1983.

Held, I. M. and Suarez, M. J.: A Proposal for the Intercomparison of the Dynamical Cores of Atmospheric General Circulation Models, Bulletin of the American Meteorological Society, 75, 1825–1830, doi:10.1175/1520-0477(1994)075<1825:APFTIO>2.0.CO;2, URL http://journals.ametsoc.org/doi/abs/10.1175/1520-0477%281994%29075%3C1825%3AAPFTIO%3E2.0.CO%3B2, 1994.

Held, I. M., Ting, M., and Wang, H.: Northern Winter Stationary Waves: Theory and Modeling, Journal of Climate, 15, 2125–2144, doi:10.1175/1520-0442(2002)015<2125:NWSWTA>2.0.CO;2, URL http://journals.ametsoc.org/doi/abs/10.1175/1520-0442%282002%29015%3C2125%3ANWSWTA%3E2.0.CO%3B2, 2002.

Hoskins, B. J. and Karoly, D. J.: The Steady Linear Response of a Spherical Atmosphere to Thermal and Orographic Forcing, J. Atmos. Sci., 38, 1179–1196, URL http://dx.doi.org/10.1175/1520-0469(1981)038<1179:TSLROA>2.0.CO;2, 1981.

Hunt, B.: Zonally symmetric global general circulation models with and without the hydrologic cycle, Tellus A, 25, URL http://www.tellusa.net/index.php/tellusa/article/view/9668, 1973.

Jia, X., Yang, S., Song, W., and He, B.: Prediction of wintertime Northern Hemisphere blocking by the NCEP Climate Forecast System, Journal of Meteorological Research, 28, 76–90, doi:10.1007/s13351-014-3085-8, URL http://dx.doi.org/10.1007/s13351-014-3085-8, 2014.

Junge, M., Blender, R., Fraedrich, K., Gayler, V., Luksch, U., and Lunkeit, F.: A world without Greenland: impacts on the Northern Hemisphere winter circulation in low- and high-resolution models, Climate Dynamics, 24, 297–307, doi:10.1007/s00382-004-0501-2, URL http://dx.doi.org/10.1007/s00382-004-0501-2, 2005.

Kalnay-Rivas, E. and Merkine, L.-O.: A Simple Mechanism for Blocking, J. Atmos. Sci., 38, 2077–2091, doi:10.1175/1520-0469(1981)038<2077:ASMFB>2.0.CO;2, URL http://dx.doi.org/10.1175/1520-0469(1981)038<2077:ASMFB>2.0.CO;2, 1981.

Koch, P., Wernli, H., and Davies, H. C.: An event-based jet-stream climatology and typology, International Journal of Climatology, 26, 283–301, doi:10.1002/joc.1255, URL http://dx.doi.org/10.1002/joc.1255, 2006.

Lejenäs, H. and Økland, H.: Characteristics of northern hemisphere blocking as determined from a long time series of observational data, Tellus A, 35A, 350–362, doi:10.1111/j.1600-0870.1983.tb00210.x, URL http://dx.doi.org/10.1111/j.1600-0870.1983.tb00210.x, 1983.

Li, C. and Wettstein, J. J.: Thermally Driven and Eddy-Driven Jet Variability in Reanalysis, J. Climate, 25, 1587–1596, URL http://dx.doi.org/10.1175/JCLI-D-11-00145.1, 2012.

Lorenz, E. N.: Deterministic Nonperiodic Flow, J. Atmos. Sci., 20, 130–141, doi:10.1175/1520-0469(1963)020<0130:DNF>2.0.CO;2, URL http://dx.doi.org/10.1175/1520-0469(1963)020<0130:DNF>2.0.CO;2, 1963.

Luo, D.: A Barotropic Envelope Rossby Soliton Model for Block—Eddy Interaction. Part I: Effect of Topography, J. Atmos. Sci., 62, 5–21, doi:10.1175/1186.1, URL http://dx.doi.org/10.1175/1186.1, 2005.

Manabe, S., Smagorinsky, J., and Strickler, R. F.: Simulated climatology of a general circulation model with a hydrologic cycle, Monthly Weather Review, 93, 769–798, 1965.

Massacand, A. C., Wernli, H., and Davies, H. C.: Heavy precipitation on the alpine southside: An upper-level precursor, Geophys. Res. Lett., 25, 1435–1438, URL http://dx.doi.org/10.1029/98GL50869, 1998.

Matsueda, M., Kyouda, M., Toth, Z., Tanaka, H. L., and Tsuyuki, T.: Predictability of an Atmospheric Blocking Event that Occurred on 15 December 2005, Mon. Wea. Rev., 139, 2455–2470, doi:10.1175/2010MWR3551.1, URL http://dx.doi.org/10.1175/2010MWR3551.1, 2011.

Mc Innes, H., Kristjánsson, J. E., Schyberg, H., and Røsting, B.: An assessment of a Greenland lee cyclone during the Greenland Flow Distortion experiment: An observational approach, Quarterly Journal of the Royal Meteorological Society, 135, 1968–1985, doi:10.1002/qj.524, URL http://dx.doi.org/10.1002/qj.524, 2009.

McCauley, M. P. and Sturman, A. P.: A Study of Orographic Blocking and Barrier Wind Development Upstream of the Southern Alps, New Zealand, Meteorology and Atmospheric Physics, 70, 121–131, doi:10.1007/s007030050029, URL http://dx.doi.org/10.1007/s007030050029, 1999.

McIntyre, M. E. and Palmer, T. N.: Breaking planetary waves in the stratosphere, Nature, 305, 593–600, URL http://dx.doi.org/10.1038/305593a0, 1983.

Moore, G. W. K. and Renfrew, I. A.: Tip Jets and Barrier Winds: A QuikSCAT Climatology of High Wind Speed Events around Greenland, J. Climate, 18, 3713–3725, URL http://dx.doi.org/10.1175/JCLI3455.1, 2005.

Nakamura, H. and Wallace, J. M.: Synoptic Behavior of Baroclinic Eddies during the Blocking Onset, Mon. Wea. Rev., 121, 1892–1903, doi:10.1175/1520-0493(1993)121<1892:SBOBED>2.0.CO;2, URL http://dx.doi.org/10.1175/1520-0493(1993)121<1892:SBOBED>2.0.CO;2, 1993.

Namias, J.: Seasonal persistence and recurrence of European blocking during 1958,Äì1960, Tellus, 16, 394–407, doi:10.1111/j.2153-3490.1964.tb00176.x, URL http://dx.doi.org/10.1111/j.2153-3490.1964.tb00176.x, 1964.

Neiman, P. J., Martin Ralph, F., Persson, P. O. G., White, A. B., Jorgensen, D. P., and Kingsmill, D. E.: Modification of Fronts and Precipitation by Coastal Blocking during an Intense Landfalling Winter Storm in Southern California: Observations during CALJET, Mon. Wea. Rev., 132, 242–273, doi:10.1175/1520-0493(2004)132<0242:MOFAPB>2.0.CO;2, URL http://dx.doi.org/10.1175/1520-0493(2004)132<0242:MOFAPB>2.0.CO;2, 2004.

Outten, S. D., Renfrew, I. A., and Petersen, G. N.: An easterly tip jet off Cape Farewell, Greenland. II: Simulations and dynamics, Quarterly Journal of the Royal Meteorological Society, 135, 1934–1949, doi:10.1002/qj.531, URL http://dx.doi.org/10.1002/qj.531, 2009.

Parish, T. R.: Barrier Winds Along the Sierra Nevada Mountains, J. Appl. Meteor., 21, 925–930, doi:10.1175/1520-0450(1982)021<0925:BWATSN>2.0.CO;2, URL http://dx.doi.org/10.1175/1520-0450(1982)021<0925:BWATSN>2.0.CO;2, 1982.

Pelly, J. L. and Hoskins, B. J.: A New Perspective on Blocking, J. Atmos. Sci., 60, 743–755, doi:10.1175/1520-0469(2003)060<0743:ANPOB>2.0.CO;2, URL http://dx.doi.org/10.1175/1520-0469(2003)060<0743:ANPOB>2.0.CO;2, 2003a.

Pelly, J. L. and Hoskins, B. J.: How well does the ECMWF Ensemble Prediction System predict blocking?, Quarterly Journal of the Royal Meteorological Society, 129, 1683–1702, doi:10.1256/qj.01.173, URL http://dx.doi.org/10.1256/qj.01.173, 2003b.

Petersen, G. N., Ólafsson, H., and Kristjánsson, J. E.: Flow in the Lee of Idealized Mountains and Greenland, Journal of the Atmospheric Sciences, 60, 2183–2195, doi:10.1175/1520-0469(2003)060<2183:FITLOI>2.0.CO;2, URL http://journals.ametsoc.org/doi/abs/10.1175/1520-0469%282003%29060%3C2183%3AFITLOI%3E2.0.CO%3B2, 2003.

Petersen, G. N., Kristjánsson, J. E., and Ólafsson, H.: Numerical simulations of Greenland's impact on the Northern Hemisphere winter circulation, Tellus A, 56, 102–111, doi:10.1111/j.1600-0870.2004.00047.x, URL http://dx.doi.org/10.1111/j.1600-0870.2004.00047.x, 2004.

Reinecke, P. A. and Durran, D. R.: Estimating Topographic Blocking Using a Froude Number When the Static Stability Is Nonuniform, J. Atmos. Sci., 65, 1035–1048, doi:10.1175/2007JAS2100.1, URL http://dx.doi.org/10.1175/2007JAS2100.1, 2008.

Renwick, J. A. and Wallace, J. M.: Relationships between North Pacific Wintertime Blocking, El Niño, and the PNA Pattern, Mon. Wea. Rev., 124, 2071–2076, doi:10.1175/1520-0493(1996)124<2071:RBNPWB>2.0.CO;2, URL http://dx.doi.org/10.1175/1520-0493(1996)124<2071:RBNPWB>2.0.CO;2, 1996.

Rex, D. F.: Blocking Action in the Middle Troposphere and its Effect upon Regional Climate: II. The Climatology of Blocking Action, Tellus, 2, 275–301, doi:10.1111/j.2153-3490.1950.tb00339.x, URL http://dx.doi.org/10.1111/j.2153-3490.1950.tb00339.x, 1950.

Ringler, T. D. and Cook, K. H.: Orographically Induced Stationary Waves: Dependence on Latitude, Journal of the Atmospheric Sciences, 52, 2548–2560, doi:10.1175/1520-0469(1995)052<2548:OISWDO>2.0.CO;2, URL http://journals.ametsoc.org/doi/abs/10.1175/1520-0469%281995%29052%3C2548%3AOISWDO%3E2.0.CO%3B2, 1995.

Ringler, T. D. and Cook, K. H.: Factors Controlling Nonlinearity in Mechanically Forced Stationary Waves over Orography, Journal of the Atmospheric Sciences, 54, 2612–2629, doi:10.1175/1520-0469(1997)054<2612:FCNIMF>2.0.CO;2, URL http://journals.ametsoc.org/doi/abs/10.1175/1520-0469%281997%29054%3C2612%3AFCNIMF%3E2.0.CO%3B2, 1997.

Rivière, G.: Effect of Latitudinal Variations in Low-Level Baroclinicity on Eddy Life Cycles and Upper-Tropospheric Wave-Breaking Processes, J. Atmos. Sci., 66, 1569–1592, doi:10.1175/2008JAS2919.1, URL http://dx.doi.org/10.1175/2008JAS2919.1, 2009.

Schär, C.: Mesoscale mountains and the larger-scale atmospheric dynamics: A review, International Geophysics, 83, 29–42, 2002.

Schär, C. and Davies, H. C.: Quasi-geostrophic stratified flow over isolated finite amplitude topography, Dynamics of Atmospheres and Oceans, 11, 287–306, URL http://www.sciencedirect.com/science/article/pii/0377026588900036, 1988.

Schwierz, C., Croci-Maspoli, M., and Davies, H. C.: Perspicacious indicators of atmospheric blocking, Geophys. Res. Lett., 31, L06 125–, URL http://dx.doi.org/10.1029/2003GL019341, 2004.

Sheppard, P. A.: Airflow over mountains, Quarterly Journal of the Royal Meteorological Society, 82, 528–529, doi:10.1002/qj.49708235418, URL http://dx.doi.org/10.1002/qj.49708235418, 1956.

Shutts, G. J.: The propagation of eddies in diffluent jetstreams: Eddy vorticity forcing of blocking flow fields, Quarterly Journal of the Royal Meteorological Society, 109, 737–761, doi:10.1002/qj.49710946204, URL http://dx.doi.org/10.1002/qj.49710946204, 1983.

Smith, R. B.: The Influence of Mountains on the Atmosphere, vol. 21 of *Advances in Geophysics*, pp. 87 – 230, Elsevier, doi:10.1016/S0065-2687(08)60262-9, URL http://www.sciencedirect.com/science/article/pii/S0065268708602629, 1979.

Smith, R. B.: Mountain-induced stagnation points in hydrostatic flow, Tellus A, 41A, 270–274, URL http://dx.doi.org/10.1111/j.1600-0870.1989.tb00381.x, 1989.

Smith, R. B. and Grønås, S.: Stagnation points and bifurcation in 3-D mountain airflow, Tellus A, 45, 28–43, doi:10.1034/j.1600-0870.1993.00003.x, URL http://dx.doi.org/10.1034/j.1600-0870.1993.00003.x, 1993.

Smolarkiewicz, P. K. and Rotunno, R.: Low Froude Number Flow Past Three-Dimensional Obstacles. Part I: Baroclinically Generated Lee Vortices, Journal of the Atmospheric Sciences, 46, 1154–1164, doi:10.1175/1520-0469(1989)046<1154:LFNFPT>2.0.CO;2, URL http://journals.ametsoc.org/doi/abs/10.1175/1520-0469%281989%29046%3C1154%3ALFNFPT%3E2.0.CO%3B2, 1989.

Snyder, W. H., Thompson, R. S., Eskridge, R. E., Lawson, R. E., Castro, I. P., Lee, J. T., Hunt, J. C. R., and Ogawa, Y.: The structure of strongly stratified flow over hills: dividing-streamline concept, Journal of Fluid Mechanics, 152, 249–288, doi:10.1017/S0022112085000684, URL http://dx.doi.org/10.1017/S0022112085000684, 1985.

Spensberger, C. and Spengler, T.: A New Look at Deformation as a Diagnostic for Large-Scale Flow, J. Atmos. Sci., 71, 4221–4234, URL http://dx.doi.org/10.1175/JAS-D-14-0108.1, 2014.

Spensberger, C., Spengler, T., and Li, C.: Upper tropospheric jet axis detection and application to the boreal winter 2013/14, Monthly Weather Review, in preparation, 2014a.

Spensberger, C., Spengler, T., and Li, C.: Wintertime variability of mid-latitude jet axes, Journal of Climate, in preparation, 2014b.

Spensberger, C., Thorsteinsson, T., and Spengler, T.: Bedymo, a combined Quasi-Geostrophy and Primitive Equation Model, Geophysical Model Development, in preparation, 2014c.

Strong, C. and Davis, R. E.: Winter jet stream trends over the Northern Hemisphere, Quarterly Journal of the Royal Meteorological Society, 133, 2109–2115, doi:10.1002/qj.171, URL http://dx.doi.org/10.1002/qj.171, 2007.

Swanson, K. L.: Stationary Wave Accumulation and the Generation of Low-Frequency Variability on Zonally Varying Flows, J. Atmos. Sci., 57, 2262–2280, URL http://dx.doi.org/10.1175/1520-0469(2000)057<2262:SWAATG>2.0.CO;2, 2000.

Swanson, K. L.: Blocking as a local instability to zonally varying flows, Quarterly Journal of the Royal Meteorological Society, 127, 1341–1355, doi:10.1002/qj.49712757412, URL http://dx.doi.org/10.1002/qj.49712757412, 2001.

Thorncroft, C. D., Hoskins, B. J., and McIntyre, M. E.: Two paradigms of baroclinic-wave life-cycle behaviour, Quarterly Journal of the Royal Meteorological Society, 119, 17–55, doi:10.1002/qj.49711950903, URL http://dx.doi.org/10.1002/qj.49711950903, 1993.

Thorsteinsson, S. and Sigurdsson, S.: Orogenic blocking and deflection of stratified air flow on an f-plane, Tellus A, 48, 572–583, doi:10.1034/j.1600-0870.1996.t01-3-00006.x, URL http://dx.doi.org/10.1034/j.1600-0870.1996.t01-3-00006.x, 1996.

Tibaldi, S. and Molteni, F.: On the operational predictability of blocking, Tellus A, 42, 343–365, doi:10.1034/j.1600-0870.1990.t01-2-00003.x, URL http://dx.doi.org/10.1034/j.1600-0870.1990.t01-2-00003.x, 1990.

Trenberth, K. E. and Chen, S.-C.: Planetary Waves Kinematically Forced by Himalayan Orography, J. Atmos. Sci., 45, 2934–2948, doi:10.1175/1520-0469(1988)045<2934:PWKFBH>2.0.CO;2, URL http://dx.doi.org/10.1175/1520-0469(1988)045<2934:PWKFBH>2.0.CO;2, 1988.

Våge, K., Spengler, T., Davies, H. C., and Pickart, R. S.: Multi-event analysis of the westerly Greenland tip jet based upon 45 winters in ERA-40, Quarterly Journal of the Royal Meteorological Society, 135, 1999–2011, doi:10.1002/qj.488, URL http://dx.doi.org/10.1002/qj.488, 2009.

Valdes, P. J. and Hoskins, B. J.: Nonlinear Orographically Forced Planetary Waves, Journal of the Atmospheric Sciences, 48, 2089–2106, doi:10.1175/1520-0469(1991)048<2089:NOFPW>2.0.CO;2, URL http://journals.ametsoc.org/doi/abs/10.1175/1520-0469%281991%29048%3C2089%3ANOFPW%3E2.0.CO%3B2, 1991.

Wallace, J., Held, I., Thompson, D., Trenberth, K., and Walsh, J.: Global Warming and Winter Weather, Science, pp. 729–730, doi:10.1126/science.343.6172.729, 2014.

Wallace, J. M. and Gutzler, D. S.: Teleconnections in the Geopotential Height Field during the Northern Hemisphere Winter, Mon. Wea. Rev., 109, 784–812, URL http://dx.doi.org/10.1175/1520-0493(1981)109<0784:TITGHF>2.0.CO;2, 1981.

Wernli, H. and Schwierz, C.: Surface Cyclones in the ERA-40 Dataset (1958–2001). Part I: Novel Identification Method and Global Climatology, J. Atmos. Sci., 63, 2486–2507, URL http://dx.doi.org/10.1175/JAS3766.1, 2006.

Wettstein, J. J. and Wallace, J. M.: Observed Patterns of Month-to-Month Storm-Track Variability and Their Relationship to the Background Flow*, J. Atmos. Sci., 67, 1420–1437, URL http://dx.doi.org/10.1175/2009JAS3194.1, 2010.

White, W. B. and Clark, N. E.: On the Development of Blocking Ridge Activity Over the Central North Pacific, J. Atmos. Sci., 32, 489–502, doi:10.1175/1520-0469(1975)032<0489:OTDOBR>2.0.CO;2, URL http://dx.doi.org/10.1175/1520-0469(1975)032<0489:OTDOBR>2.0.CO;2, 1975.

Woollings, T., Hoskins, B., Blackburn, M., and Berrisford, P.: A New Rossby Wave-Breaking Interpretation of the North Atlantic Oscillation, J. Atmos. Sci., 65, 609–626, URL http://dx.doi.org/10.1175/2007JAS2347.1, 2008.

Woollings, T., Hannachi, A., and Hoskins, B.: Variability of the North Atlantic eddy-driven jet stream, Quarterly Journal of the Royal Meteorological Society, 136, 856–868, doi:10.1002/qj.625, URL http://dx.doi.org/10.1002/qj.625, 2010.

Yu, J.-Y. and Hartmann, D. L.: Orographic Influences on the Distribution and Generation of Atmospheric Variability in a GCM, Journal of the Atmospheric Sciences, 52, 2428–2443, doi:10.1175/1520-0469(1995)052<2428:OIOTDA>2.0.CO;2, URL http://journals.ametsoc.org/doi/abs/10.1175/1520-0469%281995%29052%3C2428%3AOIOTDA%3E2.0.CO%3B2, 1995.

Zishka, K. M. and Smith, P. J.: The Climatology of Cyclones and Anticyclones over North America and Surrounding Ocean Environs for January and July, 1950–77, Mon. Wea. Rev., 108, 387–401, URL http://dx.doi.org/10.1175/1520-0493(1980)108<0387:TCOCAA>2.0.CO;2, 1980.

Appendix A

Deformation tendencies in the primitive equations and quasi-geostrophy

Introduction

The tendency equations for total deformation and the deformation angle show which physical processes can create, turn, and destroy deformation. In order to isolate the most important terms in the resulting tendency equations, I also present their equivalents within the quasi-geostrophic (QG) approximation.

The QG deformation tendencies pinpoint an important difference between the two widely adopted definitions of QG in the textbooks of Pedlosky (1986) and Holton (2004). Therefore, a brief discussion of the dynamical differences arising from the differences is required to interpret the different deformation tendencies.

Deformation tendencies

The derivation is based on the frictionless Navier-Stokes equations in z-coordinates.

$$\frac{d\boldsymbol{v}}{dt} + f\boldsymbol{k} \times \boldsymbol{v} = -\frac{1}{\rho}\nabla p \quad . \tag{A.1}$$

In this equation $\boldsymbol{v} = (u, v)$ denotes the horizontal wind vector.

Using the definitions of the deformation components $\delta_+ = u_x - v_y$ and $\delta_\times = v_x + u_y$ the tendencies for stretching deformation

$$\frac{d\delta_+}{dt} = -D\delta_+ + f\delta_\times + \beta u - \frac{1}{\rho}(p_{xx} - p_{yy}) + \frac{1}{\rho^2}(\rho_x p_x - \rho_y p_y) - (w_x u_z - w_y v_z) \tag{A.2}$$

and shearing deformation

$$\frac{d\delta_\times}{dt} = -D\delta_\times - f\delta_+ + \beta v - \frac{2}{\rho}p_{xy} + \frac{1}{\rho^2}(\rho_x p_y + \rho_y p_x) - (w_x v_z + w_y u_z) \tag{A.3}$$

follow. With the definitions of total deformation δ and the deformation angle γ

$$\delta = \sqrt{\delta_+^2 + \delta_\times^2} \tag{A.4}$$

$$\tan 2\gamma = \frac{\delta_\times}{\delta_+} \tag{A.5}$$

the time tendencies of δ and γ can be expressed in terms of the tendencies of shearing and stretching deformation,

$$\begin{aligned} \frac{\partial \delta}{\partial t} &= -\frac{1}{2\sqrt{\delta_+^2 + \delta_\times^2}}\left(2\delta_+\frac{\partial \delta_+}{\partial t} + 2\delta_\times\frac{\partial \delta_\times}{\partial t}\right) \\ &= -\frac{1}{\delta}\left(\delta_+\frac{\partial \delta_+}{\partial t} + \delta_\times\frac{\partial \delta_\times}{\partial t}\right) \end{aligned} \tag{A.6}$$

$$\begin{aligned} \frac{\partial \gamma}{\partial t} &= \frac{1}{2 + 2\frac{\delta_\times^2}{\delta_+^2}} \cdot \frac{\delta_+\frac{\partial \delta_\times}{\partial t} - \delta_\times\frac{\partial \delta_+}{\partial t}}{\delta_+^2} \\ &= \frac{1}{2\delta^2}\left[\delta_+\frac{\partial \delta_\times}{\partial t} - \delta_\times\frac{\partial \delta_+}{\partial t}\right] \end{aligned} \tag{A.7}$$

Using the tendency of total deformation as an example, the terms originating from the stretching and the shearing deformation tendencies due to advection, differential advection, divergence, and the Coriolis effect, respectively, combine into

$$\begin{aligned}\delta_+(\boldsymbol{v}\cdot\nabla\delta_+)+\delta_\times(\boldsymbol{v}\cdot\nabla\delta_\times) &= \frac{1}{2}\boldsymbol{v}\cdot\nabla\delta_+^2+\frac{1}{2}\boldsymbol{v}\cdot\nabla\delta_\times^2=\frac{1}{2}\boldsymbol{v}\cdot\nabla\delta^2\\ &= \delta\boldsymbol{v}\cdot\nabla\delta \qquad \text{(A.8)}\\ \delta_+(\boldsymbol{v}_x\cdot\nabla u-\boldsymbol{v}_y\cdot\nabla v)+\delta_\times(\boldsymbol{v}_y\cdot\nabla u+\boldsymbol{v}_x\cdot\nabla v) &= \delta_+(u_xu_x+v_xu_y-u_yv_x-v_yv_y)\\ &\quad+\delta_\times(u_yu_x+v_yu_y+u_xv_x+v_xv_y)\\ &= \delta_+^2D+\delta_\times^2D=\delta^2D \qquad \text{(A.9)}\\ \delta_+(f\delta_\times+\beta u)+\delta_\times(-f\delta_++\beta v) &= \beta(\delta_+u+\delta_\times v) \qquad \text{(A.10)}\end{aligned}$$

The pressure gradient, tilting, and solenoidal terms cannot be combined without further assumptions. The combination works analogously for the tendency of the deformation angle.

With these ingredients the deformation tendencies result in

$$\begin{aligned}\frac{d_z\ln\delta}{dt} = \overbrace{-D}^{DIV}+\frac{1}{\delta^2}\Bigg[&\overbrace{\beta(\delta_+u+\delta_\times v)}^{BETA}\overbrace{-\frac{1}{\rho}\Big(\delta_+(p_{xx}-p_{yy})+2\delta_\times p_{xy}\Big)}^{PRES}\\ &+\underbrace{\delta_+(w_xu_z-w_yv_z)+\delta_\times(w_xv_z+w_yu_z)}_{TILT}+\underbrace{\frac{1}{\rho^2}\Big(\delta_+(\rho_xp_x-\rho_yp_y)+\delta_\times(\rho_xp_y+\rho_yp_x)\Big)}_{SOL}\Bigg]\end{aligned} \qquad \text{(A.11)}$$

$$\begin{aligned}2\frac{d_z\gamma}{dt} = \overbrace{-f}^{COR}-\frac{1}{\delta^2}\Bigg[&\overbrace{\beta(\delta_\times u-\delta_+v)}^{BETA}\overbrace{-\frac{1}{\rho}\Big(\delta_\times(p_{xx}-p_{yy})-2\delta_+p_{xy}\Big)}^{PRES}\\ &+\underbrace{\delta_\times(w_xu_z-w_yv_z)-\delta_+(w_xv_z+w_yu_z)}_{TILT}+\underbrace{\frac{1}{\rho^2}\Big(\delta_\times(\rho_xp_x-\rho_yp_y)-\delta_+(\rho_xp_y+\rho_yp_x)\Big)}_{SOL}\Bigg]\end{aligned} \qquad \text{(A.12)}$$

Despite being the tendency of an absolute magnitude and an orientation, respectively, these equations are remarkably symmetric.

Physical interpretation of the tendencies

Focusing first on the pressure terms *PRES*, the patterns that optimally reinforce the respective deformation component are visualised in gray in Figure A.1a and b. They resemble the checkerboard pressure pattern that leads to frontogenesis along the axis of dilatation, which is strongest at the saddle point. By reinforcing deformation of one specific orientation, pressure turns the axis of dilatation towards this specific orientation, if the axis of dilatation was not pointing in that orientation already. Hence, a tendency in the deformation angle requires the existence of deformation perpendicular to the reinforced component.

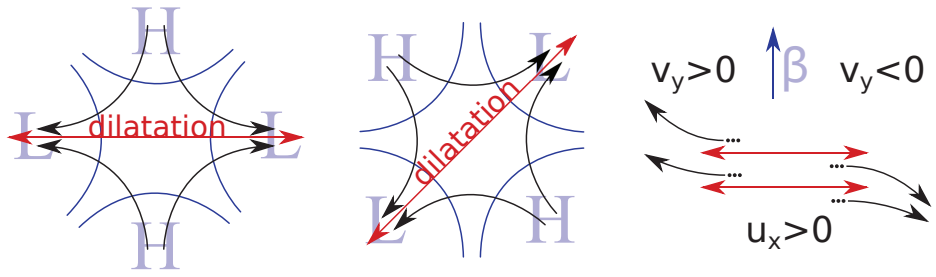

Figure A.1: Principal flow patterns (black arrows), the associated axis of dilatation (black double arrows), and favourable pressure patterns (dashed gray lines) for (a) stretching deformation and (b) shearing deformation. Panel (c) illustrates of the effect of the β-term in the deformation tendency for pure stretching deformation.

To understand the effect of the *BETA* term in (A.11), it is instructive to consider an initial state with $v = 0$ but homogeneous $u_x > 0$ corresponding to pure stretching deformation (Fig. A.1c). Then, due to the β-effect the flow further north is influenced by a stronger Coriolis force, leading to convergence (divergence) in westerly (easterly) flow. The convergence (divergence) translates into a $v_y < 0$ ($v_y > 0$) which reinforces (counteracts) the stretching deformation.

The interpretation of the remaining terms in (A.11) and (A.12) is straight-forward. Convergent flow strengthens total deformation (*DIV*), and the unbalanced part of the Coriolis force turns the axis of dilatation anti-clockwise (*COR*). The terms denoted *TILT* and *SOL* correspond to the tilting term and solenoidal term in the vorticity tendency equation.

Simplifications in Pedlosky-type quasi-geostrophy

The derivation of the deformation tendencies within the QG framework allow an assessment of the relative importance of the terms contributing to the deformation tendencies. In QG, the horizontal momentum equation is replaced by the equations

$$f_0 \boldsymbol{k} \times \boldsymbol{v}_g = -\frac{1}{\rho_0} \nabla_z p_g \tag{A.13}$$

$$\frac{d_{gz} \boldsymbol{v}_g}{dt} + f_0 \boldsymbol{k} \times \boldsymbol{v}_a + \beta y \boldsymbol{k} \times \boldsymbol{v}_g = -\frac{1}{\rho_0} \nabla_z p_a \tag{A.14}$$

in which the subscripts g and a stand for the geostrophic and ageostrophic parts, respectively. In the derivation, we use the β-plane and Boussinesq approximations (Pedlosky,

1986). The resulting tendencies are

$$\frac{d_{zg}\ln\delta_g}{dt} = \frac{1}{\delta_g^2}\left[\beta(\delta_{+g}u_a + \delta_{\times g}v_a) - \frac{1}{\rho_0}\Big(\delta_{+g}(p_{axx} - p_{ayy}) + 2\delta_{\times g}p_{axy}\Big)\right] \tag{A.15}$$

$$2\frac{d_{zg}\gamma_g}{dt} = -\beta y - \frac{1}{\delta_g^2}\left[\beta(\delta_{\times g}u_a - \delta_{+g}v_a) - \frac{1}{\rho_0}\Big(\delta_{\times g}(p_{axx} - p_{ayy}) - 2\delta_{+g}p_{axy}\Big)\right] \tag{A.16}$$

Compared to the full primitive equation version of the tendencies, the solenoidal and the tilting terms are neglected because of the Boussinesq approximation and the small vertical velocities, respectively. The pressure terms take the same form as in the full primitive equation version, but are based on the ageostrophic pressure alone, indicating that the geostrophic parts of the pressure terms cannot influence deformation. This indication can be proven by using (A.13) to rewrite $p_{gxx} - p_{gyy}$ as $\rho_0 f_0 \delta_{\times g}$ and $2p_{gxy}$ as $\rho_0 f_0 \delta_{+g}$. With those substitutions the geostrophic parts of the *PRES* terms cancel also in the primitive equation version of the deformation tendency (A.11). In the tendency of the deformation angle (A.12) the geostrophic pressure terms combine to $+f_0$ and hence largely balance the *COR* term $-f$. This cancellation leads to the $-\beta y$-contribution in the QG tendency of the deformation angle.

Simplifications in Holton-type quasi-geostrophy

Expanding only the wind velocity components in orders of the Rossby number results in a further simplification of the equations, because there are no ageostrophic pressure gradients (e.g. Holton, 2004).

$$\frac{d_{zg}\ln\delta_g}{dt} = \frac{\beta}{\delta_g^2}(\delta_{+g}u_a + \delta_{\times g}v_a) \tag{A.17}$$

$$2\frac{d_{zg}\gamma_g}{dt} = -\beta y - \frac{\beta}{\delta_g^2}(\delta_{\times g}u_a - \delta_{+g}v_a) \tag{A.18}$$

Hence, on an f-plane, both the total deformation and the deformation angle are conserved.

Albeit leading to the same vorticity tendencies, the different set of QG equations presented by Pedlosky (1986) and Holton (2004) lead to important differences in the deformation tendencies. However, as the vorticity tendency fully determines the evolution of the geostrophic flow field, the geostrophic deformation tendencies must be equal in both systems, if they are initialised with equal geostrophic vorticity. The contribution of the pressure terms must consequently be counterbalanced by the β-terms or vanish on an f-plane.

Apart from the inconsistency in the deformation tendencies, there are further important differences between the QG definitions of Holton (2004) and Pedlosky (1986). Comparing, for example, the geostrophic divergence tendencies, which in both cases

must equal zero,

$$u_{gx}^2 + v_{gx}u_{gy} + u_{gy}v_{gx} + v_{gy}^2 + f_0\zeta_a - \beta u_g + \beta y\zeta_g = -\frac{1}{\rho_0}\nabla^2 p_a \quad \text{(Pedlosky)} \quad \text{(A.19)}$$

$$u_{gx}^2 + v_{gx}u_{gy} + u_{gy}v_{gx} + v_{gy}^2 + f_0\zeta_a - \beta u_g + \beta y\zeta_g = 0 \quad \text{(Holton)} \quad \text{(A.20)}$$

The first four terms can be rewritten as $2\psi_{gxy}^2 - 2\psi_{gxx}\psi_{gyy}$. Also, $2\psi_{gxy}^2 = \frac{1}{2}\delta_{+g}^2$ and $-2\psi_{gxx}\psi_{gyy} = \frac{1}{2}\delta_{\times g}^2 - \frac{1}{2}\zeta_g^2$. The first four terms are thus the Okubo-Weiss parameter $\frac{1}{2}\delta_g^2 - \frac{1}{2}\zeta_g^2$, evaluated using the geostrophic wind components Okubo (1970); Weiss (1991).

These equations allow us to gain further insight into the role of the ageostrophic geopotential in QG dynamics. To clarify the argument, the beta terms are omitted in the following. Following Pedlosky (1986), the divergence tendency reduces to

$$\frac{1}{2}\delta_g^2 - \frac{1}{2}\zeta_g^2 + f_0\zeta_a = -\frac{1}{\rho_0}\nabla^2 p_a \quad . \quad \text{(A.21)}$$

Hence, a non-zero Okubo-Weiss parameter must be balanced by either a rotating ageostrophic wind, or an ageostrophic geopotential. Consequently, the Okubo-Weiss parameter shows the amount of cancellation between the ageostrophic vorticity and the ageostrophic geopotential. For pure shear flow, when the Okubo-Weiss parameter is exactly zero, the relation reduces to a geostrophic balance for the ageostrophic geopotential. Such a relation would be, in my opinion, albeit mathematically valid and consistent, not physically meaningful. In this case, ζ_a could—and should—be added to ζ_g, because that results in a smaller Rossby number and thus an overall better approximation of the primitive equations. The same argument applies for a non-zero Okubo-Weiss parameter, which does not rule out cancellation effects between the ageostrophic vorticity and the ageostrophic geopotential.

A simple way to avoid any cancellation is to use the additional degree of freedom in the Pedlosky (1986) definition of quasi-geostrophy to require either $\zeta_a = 0$ or $\nabla^2 p_a = 0$. As these requirements make a partial geostrophic balance in the ageostrophic circulation impossible, they also ensure an optimally low Rossby number and hence an optimal approximation of the primitive equations.

One of the optimal choices is to set $\nabla^2 p_a = 0$, showing that the Holton (2004) definition of QG is one of the optimal limits of the Pedlosky (1986) definition. Hence, the simpler quasi-geostrophic deformation tendencies (Eqs. A.17, A.18) following from the Holton (2004) definition are at least as good an approximation to the their primitive-equation equivalents as the ones following from Pedlosky (1986). As a consequence, to a good approximation, quasi-geostrophic deformation is conserved on an f-plane.

Bibliography

Holton, J. R.: Dynamic Meteorology, Elsevier Academic Press, 2004.

Okubo, A.: Horizontal dispersion of floatable particles in the vicinity of velocity singularities such as convergences, Deep Sea Research and Oceanographic Abstracts, 17, 445 – 454, doi:10.1016/0011-7471(70)90059-8, URL http://www.sciencedirect.com/science/article/pii/0011747170900598, 1970.

Pedlosky, J.: Geophysical Fluid Dynamics, Springer New York, 1986.

Weiss, J.: The dynamics of enstrophy transfer in two-dimensional hydrodynamics, Physica D: Nonlinear Phenomena, 48, 273 – 294, doi:10.1016/0167-2789(91)90088-Q, URL http://www.sciencedirect.com/science/article/pii/016727899190088Q, 1991.

Appendix B

BEDYMO: Concept and derivation of the model equations

Introduction

The "BErgen DYnamic MOdel" (BEDYMO) is an idealised regional atmospheric model. The main aim with the development of BEDYMO is to be able to study effects of the lower boundary, such as orographic blocking or ocean–atmosphere heat fluxes, in an idealised framework. The basic concepts for the model formulation hence aim for an accurate representation of lower boundary effects.

Motivation and Background

Lower boundary effects have a profound influence on both weather an climate. For example, orography has an important impact on the development of synoptic systems (e.g. Zishka and Smith, 1980; Wallace et al., 1988; Egger et al., 2014). In particular, orography can induce or strengthen cyclogenesis in the lee (e.g. Egger, 1988; Bannon, 1992; Egger, 1995). Furthermore, contrasts in the surface properties can influence weather on meso- and larger scales. Along the North American east coast, the contrast between the cold land and the warm ocean regularly leads coastal fronts in fall and winter (Riordan, 1990; Srock and Bosart, 2009). Also, the surface temperature contrast between sea-ice covered and open ocean can have dynamical implications Langland et al. (1989); Papritz et al. (2014).

On climatological time scales, orography and other inhomogeneities of the surface characteristics lead to the observed zonal asymmetries of the atmospheric circulation. These asymmetries show, that the lower surface strongly affects not only the individual cyclone, but also the storm track, and the jet structure as a whole. For example, the preferred locations of cyclogenesis in the lee of orography anchor the storm track and hence lead to preferred locations for dynamic blocking (e.g. Egger, 1978; Swanson, 2001; Luo, 2005). These preferred locations for blocking are well-documented in blocking climatologies (e.g. Pelly and Hoskins, 2003; Schwierz et al., 2004; Barriopedro et al., 2006) and influence the local climate. Furthermore, blocking orography can act as a temperature barrier, thereby altering the climatological temperature distribution. For example, Greenland shields the comparatively warm North Atlantic from the cold ice-covered Labrador sea associated with the climatological cold pool over the Canadian Arctic. A hypothetical removal of Greenland would thus strongly affect the Climate in Central Europe and Scandinavia (Petersen et al., 2004; Junge et al., 2005).

To be able to better understand the dynamics underlying these interactions between the lower surface, orographic blocks, dynamic blocks, and jet streams, we have to resort to idealised modelling. The potential mechanisms and feed backs are too complex to be

understood based on measurements or the simulation of realistic case studies alone (e.g Parish, 1982; McCauley and Sturman, 1999; Mc Innes et al., 2009; Outten et al., 2009). The relative importance of most interactions is unclear. Hence it is a-priori unknown, which approximation to the full atmospheric dynamics is most appropriate to describe the interactions. Furthermore, the appropriate approximation will depend on which aspect of the flow–orography interaction is under consideration. While non-linear quasi-geostrophy (QG) might already include the most relevant dynamics of lee cyclogenesis, the simulation of sharp fronts along ice edges will likely require semi-geostrophic (SG) dynamics in which also the ageostrophic flow contributes to the sharpening of the front. Along steep orography, the flow might be accelerated fast enough to invalidate the assumption of balanced flow in QG and SG. Hence, these situations can only be simulated appropriately using the primitive equations (PE).

Required features for BEDYMO

Consequently, in addition to representing the lower boundary condition accurately, BEDYMO should include several approximations and allow to easily switch between them. The ability to switch between approximations would allow BEDYMO to represent the dynamics of many aspects of flow–orography interaction in their respective simplest manifestation. Furthermore, the switch allows to directly compare the representation of these aspects in different approximations. To keep the comparison as straight-forward as possible, the different approximations should be solved as consistently as possible.

The comparison of different approximation is otherwise only possible by comparing different models. The comparison of different models complicates the comparison of the actual dynamics, because additional differences can arise due to the different numerics, different treatment of boundaries, and subtle differences in the model setup. Furthermore, the typical approaches to numerically solve the QG, SG, and PE system differ considerably. For example, QG models typically forecast the QG potential vorticity (QGPV) and diagnose the geostrophic wind that is required for the time integration by inverting the defining equation of QGPV (e.g. Charney and Phillips, 1953). The equivalent approach is not feasible for solving the dry hydrostatic primitive equations (PE), because in PE, the wind velocity components need be able to evolve independently from the temperature distribution.

Furthermore, BEDYMO should not use terrain-following coordinates, because they hide the volume-blocking effect of orography in the coordinate system. With terrain-following coordinates, orography affects the entire atmospheric column above orographic slopes, because it introduces pressure gradients along the tilted coordinate surface. These pressure gradients needs to be largely compensated through the introduction of an additional counteracting force to the momentum equations. A terrain-intersecting vertical coordinate avoids these problems at the expense of a more complicated lower boundary condition. In this representation, orography can only directly affect the flow in those grid cell that actually intersect with orography. While the difference between these different coordinate systems naturally has to vanish for very small grid spaces and time steps, we expect our terrain-intersecting coordinates to be more

accurate for the intended use of idealised simulations on comparatively coarse vertical grids.

To our knowledge, there is no model that combines several approximations in one framework. Furthermore, most idealised atmospheric models use pressure-based terrain-following coordinates, often denoted as σ-coordinates. To fill this gap, we devised BEDYMO, that combines these two features.

There are several options for orography-intersecting coordinate systems. We chose to use cartesian z-coordinates rather than a pressure-based vertical coordinate, because changes in the surface pressure imply changes in the extent of the blocked part of the model domain. Hence, all information concerning the blocking of grid cells would need to be updated every time step, thereby unnecessarily complicating the time integration.

Starting a new model development from scratch has a few more positive side effects, because many QG, SG, and PE models have originally been devised in the 1980ies and 1990ies (e.g. Table 1 of Schär and Wernli, 1993). By starting from scratch, we can more easily adopt some comparatively new features of Fortran 95 and 2003 that help the modularity, readability, and hence maintainability of the source code. In addition, the source code is organised in a way to make it easily accessible from python. Besides allowing for flexible yet easy-to-read run scripts, the python bindings provide the basis for a graphical user interface (GUI) which allows to interactively run the model and watch the flow evolution “live" while the model is running. All these features make BEDYMO an ideal tool not only for research but also for teaching and for student’s projects.

Model physics

Our common approach to solve the quasi-geostrophic, semi-geostrophic, and the dry, hydrostatic primitive equations is based on the thermodynamic equation, because the equation is only subject to small modifications between the approximations. The only differences are the wind velocity components used in the advection terms (Tab. B.1). In conjunction with a lower boundary condition provided by the forecasted surface pressure, the temperature distribution fully determines the atmospheric state in the QG and SG systems. In PE, the horizontal wind velocity components evolve independently and must hence be forecasted as well.

Derivation of the basic model equations

We start from the hydrostatic primitive equations in z-coordinates. In order to provide an energy sink for long and short waves, respectively, the momentum equations include scale-inselective Ekman friction and a scale-selective damping term that relax the wind velocities towards the unperturbed initial state, indicated by the δ-operator.

$$\frac{\partial \boldsymbol{v}}{\partial t} + \boldsymbol{v} \cdot \nabla_h \boldsymbol{v} + w\frac{\partial \boldsymbol{v}}{\partial z} + f\boldsymbol{k} \times \boldsymbol{v} = -\frac{1}{\rho}\nabla_h p - r\delta\boldsymbol{v} + D\nabla^2\delta\boldsymbol{v} \tag{B.1}$$

$$\frac{\partial p}{\partial z} = -\rho g \tag{B.2}$$

$$\frac{\partial \rho}{\partial t} + \nabla_h(\rho \boldsymbol{v}) + \frac{\partial \rho w}{\partial z} = 0 \tag{B.3}$$

$$\frac{\partial T}{\partial t} + \boldsymbol{v} \cdot \nabla_h T + w\frac{\partial T}{\partial z} - \frac{1}{c_p \rho}\frac{dp}{dt} = \frac{J}{c_p} \tag{B.4}$$

$$p = \rho R T \tag{B.5}$$

In this set of equations, $\boldsymbol{v}$ is the horizontal wind velocity vector, w is the vertical wind, f is the spatially varying Coriolis parameter, ρ is density, p is pressure, g the gravitational acceleration close to the Earth surface, T is temperature, c_p is the isobaric specific heat of dry air, J is the heating rate, and R is the gas constant for dry air.

As a first step, we express the total pressure tendency in (B.4) in terms of the vertical

Table B.1: Summary of the common approach to solve the QG, SG, and PE systems. Prognostic equations are marked bold. In this table, u and v denote advecting wind velocities.

Variable	QG	SG	PE
T	**Eq. (B.27)**	**Eq. (B.40)**	**Eq. (B.18)**
p_s	**Eq. (B.39), (B.37)**	**Eqs. (B.39), (B.41)**	**Eqs. (B.22)**
u, v	$=(u_g, v_g)$	$=(u_g+u_a, v_g+v_a)$	**Eq. (B.15)**
p'	Eq. (B.16)	Eq. (B.16)	Eq. (B.16)
u_g, v_g	Eq. (B.24)	Eq. (B.24)	
u_a, v_a		Eq. (B.53)	
w	Eq. (B.31)	Eq. (B.53)	Eq. (B.17)

wind w by using the hydrostatic equation.

$$\begin{aligned}\frac{dp}{dz} &= \frac{\partial p}{\partial z} + \frac{dt}{dz}\frac{\partial p}{\partial t} + \frac{dx}{dt}\frac{dt}{dz}\frac{\partial p}{\partial x} + \frac{dy}{dt}\frac{dt}{dz}\frac{\partial p}{\partial y} \\ &= \frac{\partial p}{\partial z} + \frac{1}{w}\frac{\partial p}{\partial t} + \frac{u}{w}\frac{\partial p}{\partial x} + \frac{v}{w}\frac{\partial p}{\partial y} \qquad \text{(B.6)} \\ &\approx \frac{\partial p}{\partial z} \qquad \text{(B.7)}\end{aligned}$$

It follows that

$$\frac{1}{\rho}\frac{dp}{dt} \approx -gw \quad . \qquad \text{(B.8)}$$

BEDYMO only simulates the deviations from a stationary, hydrostatic basic state with $\rho_0 = \rho_0(z)$, $p_0 = p_0(z)$. Based on these assumptions, it follows that $T_0 = T_0(z)$, $\phi_0 = \phi_0(z)$ and $\psi_0 = \psi_0(z)$. With those relations, the primitive equations take the form

$$\frac{\partial \boldsymbol{v}}{\partial t} + \boldsymbol{v}\cdot\nabla_h\boldsymbol{v} + w\frac{\partial \boldsymbol{v}}{\partial z} + f\boldsymbol{k}\times\boldsymbol{v} = -\frac{1}{\rho}\nabla_h p - r\delta\boldsymbol{v} + D\nabla^2\delta\boldsymbol{v} \qquad \text{(B.9)}$$

$$\frac{\partial p'}{\partial z} = -\rho' g \qquad \text{(B.10)}$$

$$\frac{\partial \rho'}{\partial t} + \nabla_h(\rho\boldsymbol{v}) + \frac{\partial \rho w}{\partial z} = 0 \qquad \text{(B.11)}$$

$$\frac{\partial T'}{\partial t} + \boldsymbol{v}\cdot\nabla_h T' + \left(\frac{\partial T}{\partial z} + \frac{g}{c_p}\right)w = \frac{J}{c_p} \qquad \text{(B.12)}$$

$$p' = \rho' R T_0 + \rho R T' \qquad \text{(B.13)}$$

Applying the anelastic approximation, we assume $\rho_0 \gg \rho'$ such that $\rho = \rho_0 + \rho' \approx \rho_0$. We furthermore neglect the local time tendency $\frac{\partial \rho'}{\partial t} \approx 0$, eliminating sound waves. As in the Boussinesq approximation, the approximated version of the ideal gas law

$$\frac{p'}{p_0} = \frac{\rho'}{\rho_0} + \frac{T'}{T_0} \qquad \text{(B.14)}$$

along with the observation that generally $\frac{\delta p}{p} < \frac{\delta T}{T}$ suggests the relation $\frac{T'}{T_0} \approx -\frac{\rho'}{\rho_0}$ between temperature and density perturbations. Hence, also for temperature, $T \approx T_0$.

$$\frac{\partial \boldsymbol{v}}{\partial t} + \boldsymbol{v} \cdot \nabla_h \boldsymbol{v} + w\frac{\partial \boldsymbol{v}}{\partial z} + f\boldsymbol{k} \times \boldsymbol{v} = -\frac{1}{\rho_0}\nabla_h p' - r\delta\boldsymbol{v} + D\nabla^2\delta\boldsymbol{v} \tag{B.15}$$

$$\frac{\partial p'}{\partial z} = \rho_0 g\frac{T'}{T_0} \tag{B.16}$$

$$\nabla_h \cdot \boldsymbol{v} + \frac{1}{\rho_0}\frac{\partial \rho_0 w}{\partial z} = 0 \tag{B.17}$$

$$\frac{\partial T'}{\partial t} + \boldsymbol{v} \cdot \nabla_h T' + \left(\frac{\partial T_0}{\partial z} + \frac{g}{c_p}\right) w = \frac{J}{c_p} \tag{B.18}$$

In this system, the surface pressure tendency

$$\begin{aligned}\frac{\partial p_s}{\partial t} &= g\int_{z_{top}}^{z_s} \frac{\partial \rho}{\partial t} dz = -g\int_{z_{top}}^{z_s} \nabla \cdot (\rho \boldsymbol{v}) dz \\ &= -g\int_{z_{top}}^{z_s} \nabla \cdot (\rho_0 \boldsymbol{v}) dz - g\int_{z_{top}}^{z_s} \nabla \cdot (\rho' \boldsymbol{v}) dz \\ &= g(\rho_0 w)_{top} - \frac{g}{T_0}\int_{z_{top}}^{z_s} \rho_0 \frac{\partial T'}{\partial t} dz\end{aligned} \tag{B.19}$$

is given by the mass flux convergence using the basic state density and the mass-weighted mean temperature tendency in the column.

The temperature tendency in (B.19) implies that a column-integrated temperature tendency can change the total air mass in the column, thereby violating mass conservation. To make sure the model is mass-conserving, we enforce the mass continuity also for the density perturbations by

$$\frac{\rho_0}{T_0}\frac{\partial T'}{\partial t} = \frac{\partial \rho'}{\partial t} = -\frac{\partial \rho_0 w_{exp}}{\partial z} \quad , \tag{B.20}$$

such that the expansion of the air column, reflected in w_{exp}, contributes to the vertical velocity used in (B.19). Hence, we can express the temperature contribution in (B.19) as

$$\frac{g}{T_0}\int_{z_{top}}^{z_s} \rho_0 \frac{\partial T'}{\partial t} dz = -g\int_{z_{top}}^{z_s} \frac{\partial \rho_0 w_{exp}}{\partial z} dz = -g(\rho_0 w_{exp})_{top} \quad , \tag{B.21}$$

showing that the temperature term exactly cancels the additional vertical velocity due to thermal expansion. Consequently, enforcing mass continuity for density perturbations is equivalent to omitting the temperature tendency from (B.19). Hence, the surface pressure tendency in BEDYMO is simply

$$\frac{\partial p_s}{\partial t} = g(\rho_0 w)_{top} \quad . \tag{B.22}$$

The equations (B.15)–(B.18) and (B.22) form a closed set. The only unknown parameters in the prognostic equations for temperature, surface pressure, and the horizontal wind velocity components are the perturbation pressure and p' and the vertical

velocity w. We diagnose them by integrating hydrostasy (B.16) and the continuity equation (B.17) upwards. The value of p' at the lower boundary is given by the surface pressure p_s, the value of w follows the boundary condition

$$w_s = \boldsymbol{v}_s \cdot \nabla_h z_s \quad , \tag{B.23}$$

respectively. The horizontal wind vector at the lower surface $\boldsymbol{v}_s$ is taken to be equal to the horizontal wind vector at the lowest model level.

Simplifications for Quasi-Geostrophy

To introduce QG, we define a geostrophic wind $\boldsymbol{v}_g$, which geostrophically balances the pressure gradient,

$$f_0 \boldsymbol{k} \times \boldsymbol{v}_g = -\frac{1}{\rho_0} \nabla p' = -\nabla \phi' \quad . \tag{B.24}$$

Deviations from this balance are accounted for by the ageostrophic wind $\boldsymbol{v}_a = \boldsymbol{v} - \boldsymbol{v}_g$. We also define the constant parameter β for deviations from f_0 using the β-plane approximation, $f = f_0 + \beta y$.

With these definitions, the thermodynamic equation (B.18) and the momentum equations (B.15) become

$$\frac{\partial T'}{\partial t} + (\boldsymbol{v}_g + \boldsymbol{v}_a) \cdot \nabla_h T' + w \left(\frac{\partial T_0}{\partial z} + \frac{g}{c_p} \right) = \frac{J}{c_p} \tag{B.25}$$

$$\begin{aligned} \frac{\partial \zeta_g + \zeta_a}{\partial t} &+ (\boldsymbol{v}_g + \boldsymbol{v}_a) \cdot \nabla_h (\zeta_g + \zeta_a) - (f_0 + \zeta_g + \zeta_a) \frac{1}{\rho_0} \frac{\partial \rho_0 w}{\partial z} \\ &+ \boldsymbol{k} \cdot \left(\frac{\partial \boldsymbol{v}_g + \boldsymbol{v}_a}{\partial z} \times \nabla_h w \right) + \beta (v_g + v_a) = -r \delta \zeta_g + D \nabla^2 \delta \zeta_g \quad . \end{aligned} \tag{B.26}$$

We assume the scales $U_a = Ro\,U$, $\beta L = Ro\,f$, a δT-scale for T', and a divergence scale from the continuity equation (B.17) as $\frac{W}{H} = Ro \frac{U}{L}$. Retaining only the $(\frac{U^2}{L^2})$-terms in the vorticity tendency, and the $(\delta T \frac{U}{L})$-terms in the thermodynamic tendency, the equations (B.25) and (B.26) reduce to

$$\frac{\partial T'}{\partial t} + \boldsymbol{v}_g \cdot \nabla_h T' + w \left(\frac{\partial T_0}{\partial z} + \frac{g}{c_p} \right) = \frac{J}{c_p} \quad , \tag{B.27}$$

$$\frac{\partial \zeta_g}{\partial t} + \boldsymbol{v}_g \cdot \nabla_h \zeta_g - \frac{f_0}{\rho_0} \frac{\partial \rho_0 w}{\partial z} + \beta v_g = -r \delta \zeta_g + D \nabla^2 \delta \zeta_g \quad . \tag{B.28}$$

In QG, we integrate the thermodynamic equation (B.27), and use the vertical integral of the vorticity equation (B.28) to forecast surface pressure. We only need to determine the vertical velocity to close the system of equations. We determine w by inverting the QG omega-equation.

To derive the omega-equation, we use hydrostasy $T' = \frac{T_0}{g} \frac{\partial \phi'}{\partial z}$, and the definition of the (geostrophic) geopotential $\nabla_h^2 \phi' = f_0 \zeta_g$, to rewrite equations (B.27) and (B.28) in

terms of the geopotential,

$$\left[\frac{\partial}{\partial t}+\boldsymbol{v}_g\cdot\nabla_h\right]\left(\frac{\partial\nabla_h^2\phi'}{\partial z}\right)+(\nabla_h^2\boldsymbol{v}_g)\cdot\nabla_h\frac{\partial\phi'}{\partial z}+N^2\nabla_h^2 w=\nabla_h^2 J^* \quad , \tag{B.29}$$

$$\left[\frac{\partial}{\partial t}+\boldsymbol{v}_g\cdot\nabla_h\right]\left(\frac{\partial\nabla_h^2\phi'}{\partial z}\right)+\frac{\partial\boldsymbol{v}_g}{\partial z}\cdot\nabla_h(\nabla_h^2\phi'+f_0 f)-\frac{\partial}{\partial z}\left(\frac{1}{\rho_0}\frac{\partial\rho_0 w}{\partial z}\right)= \\ =-r\nabla_h\frac{\partial\delta\phi'}{\partial z}+D\nabla_h\frac{\partial\nabla_h^2\delta\phi'}{\partial z} \quad . \tag{B.30}$$

By combining these equations, the geopotential tendency can be eliminated to yield a z-coordinate version of the omega-equation,

$$\left[N^2\nabla_h^2+f_0^2\rho_0\frac{\partial}{\partial z}\left(\frac{1}{\rho_0}\frac{\partial}{\partial z}\right)\right](\rho_0 w)= \\ =\rho_0\left[\frac{\partial\boldsymbol{v}_g}{\partial z}\cdot\nabla_h(\nabla_h^2\phi'+f_0 f)-(\nabla_h^2\boldsymbol{v}_g)\cdot\nabla_h\frac{\partial\phi'}{\partial z}+\nabla_h^2 J^*+r\frac{\partial\nabla_h^2\delta\phi'}{\partial z}-D\nabla_h^2\frac{\partial\nabla_h^2\delta\phi'}{\partial z}\right] \\ =\rho_0\nabla_h\cdot\left[\frac{\partial}{\partial z}\left(\boldsymbol{v}_g(\nabla_h^2\phi'+f_0 f)\right)+\nabla_h\left(-(\nabla^2\boldsymbol{v}_g)\cdot\frac{\partial\phi'}{\partial z}+J^*+r\frac{\partial\delta\phi'}{\partial z}-D\frac{\partial\nabla_h^2\delta\phi'}{\partial z}\right)\right] \\ =\rho_0\nabla_h\cdot\boldsymbol{Q} \quad . \tag{B.31}$$

The omega-equation only contains the vertical derivative of the vorticity equation, such that the three-dimensional balance established by the omega-equation only contains the baroclinic part of the total QG balance (for a further discussion of this problem see Keyser et al., 1989; Xu and Keyser, 1993). The barotropic part of the QG balance must hence be established separately. We use the vertically averaged vorticity tendency equation for that purpose, forecasting the surface pressure change due to barotropic motions.

We hence split the surface pressure into a barotropic p_b and a baroclinic p_s^* component $p_s=p_b+p_s^*$. The baroclinic tendency reflects the column integrated temperature change

$$<T'>=\frac{1}{\overline{\rho}_0 H}\int_{z_{top}}^{z_s}\rho_0 T' dz \tag{B.32}$$

where $H=z_{top}-z_s$ the height of the domain and $\overline{\rho}_0$ the average basic state density. From the thermal wind relation,

$$p_s^*-p_{top}^*=\overline{\rho}_0 H<T'>=\int_{z_{top}}^{z_s}\rho_0 T' dz \quad . \tag{B.33}$$

To solve this equation, we need another relation between p_s^* and p_{top}^*. We obtain such a relation by ensuring that the baroclinic circulation does not project on the barotropic wind velocities. In other word, we require the column-average baroclinic wind velocity components to vanish,

$$<u^*>=<v^*>=0 \quad , \tag{B.34}$$

where the angle brackets are defined analogously to the column-averaged temperature $<T'>$. Solving these relations by integrating the thermal wind relation upwards gives

$$\frac{\partial p_s^*}{\partial y}=-\frac{g}{HT_0}\int_{z_{top}}^{z_s}\int_{z_{top}}^{z}\rho_0\frac{\partial T'}{\partial y}dz^2 \quad , \tag{B.35}$$

and an analogous relation for $\frac{\partial p_s^*}{\partial x}$. Hence,

$$p_s^* = -\frac{g}{HT_0}\int_{z_{top}}^{z_s}\int_{z_{top}}^{z}\rho_0 T' dz^2 + C \tag{B.36}$$

where the integration constant C amounts to a pressure offset that has no effect in the model, and that hence can safely be set to zero.

The barotropic circulation can be inferred from the column-integrated vorticity equation

$$\frac{\partial <\zeta_g>}{\partial t} + <\boldsymbol{v}_g\cdot\zeta_g> - \frac{f}{\overline{\rho}_0}[\rho_0 w]_{z_s}^{z_{top}} + \beta <v_g> = -r\delta <\zeta_g> + D\nabla^2\delta <\zeta_g> \quad . \tag{B.37}$$

The barotropic component of the surface pressure can then be obtained by inverting

$$\frac{1}{\overline{\rho}_0}\nabla^2 p_b = f_0 <\zeta_g> \quad . \tag{B.38}$$

Hence, the total surface pressure tendency results in

$$\frac{\partial p_s}{\partial t} = \nabla^{-2}\frac{\partial (f <\zeta_g>)}{\partial t} - \frac{g}{(z_{top}-z_s)T_0}\int_{z_{top}}^{z_s}\int_{z_{top}}^{z}\rho_0 T' dz^2 \quad . \tag{B.39}$$

Simplifications in Semi-Geostrophy

The same procedure as in QG can be used, except that also $(Ro\frac{U}{L})$-terms are retained. The resulting thermodynamic equation and the resulting barotropic vorticity tendency are

$$\frac{\partial T'}{\partial t} + (\boldsymbol{v}_g + \boldsymbol{v}_a)\cdot\nabla_h T' + w\left(\frac{\partial T_0}{\partial z} + \frac{g}{c_p}\right) = \frac{J}{c_p} \quad \text{and} \tag{B.40}$$

$$\frac{\partial <\zeta_g>}{\partial t} + <(\boldsymbol{v}_g + \boldsymbol{v}_a)\cdot\nabla\zeta_g> - \frac{f_0 + <\zeta_g>}{\overline{\rho}_0}[\rho_0 w]_{z_s}^{z_{top}} + \beta <v_g + v_a> = \\ = -r\delta <\zeta_g> + D\nabla^2\delta <\zeta_g> \quad . \tag{B.41}$$

In the derivation of the diagnostics, we will also use the SG momentum equation

$$\frac{\partial \boldsymbol{v}_g}{\partial t} + (\boldsymbol{v}_g + \boldsymbol{v}_a)\cdot\nabla_h\boldsymbol{v}_g + f\boldsymbol{k}\times(\boldsymbol{v}_g + \boldsymbol{v}_a) = -\frac{1}{\rho_0}\nabla p' - r\delta\boldsymbol{v}_g + D\nabla^2\delta\boldsymbol{v}_g \quad . \tag{B.42}$$

In addition to a diagnostic equation for the vertical velocity w, also diagnostics for the ageostrophic horizontal velocity components are necessary to solve the system. Following the procedure of Xu (1990), we introduce a stream function vector $\boldsymbol{\psi}_a =$

$(\psi_{a1}, \psi_{a2}, \psi_{a3})$ defining the 3D ageostrophic wind $\boldsymbol{u}_a = (u_a, v_a, w)$ by

$$u_a = \frac{1}{\rho_0}\frac{\partial \rho_0 \psi_{a2}}{\partial z} - \frac{\partial \psi_{a3}}{\partial y} \quad , \tag{B.43}$$

$$v_a = \frac{\partial \psi_{a3}}{\partial x} - \frac{1}{\rho_0}\frac{\partial \rho_0 \psi_{a1}}{\partial z} \quad , \tag{B.44}$$

$$w = \frac{\partial \psi_{a1}}{\partial y} - \frac{\partial \psi_{a2}}{\partial x} \quad , \tag{B.45}$$

which can be determined diagnostically. The first step to derive relations for the components of $\boldsymbol{\psi}_a$ is to realise that we can recast the SG momentum (B.42) and the SG thermodynamic equation (B.40) as

$$D_g \nabla \phi' + \mathcal{L}\boldsymbol{u}_a = \mathcal{B}(\boldsymbol{v}_g) \tag{B.46}$$

with $D_g = \left(\frac{\partial}{\partial t} + \boldsymbol{v}_g \cdot \nabla_h\right)$ the geostrophic total derivative and a matrix $\mathcal{L}$. The function $\mathcal{B}$ contains the β-effect, the heating terms, and friction. The entries in $\mathcal{L}$ are

$$\begin{aligned}
\mathcal{L}_{11} &= f_0 \partial_x v_g + f_0 f \quad , \\
\mathcal{L}_{22} &= -f_0 \partial_y u_g + f_0 f \quad , \\
\mathcal{L}_{33} &= N^2 \quad , \\
\mathcal{L}_{12} = \mathcal{L}_{21} &= f_0 \partial_y v_g = -f_0 \partial_x u_g \quad , \\
\mathcal{L}_{13} = \mathcal{L}_{31} &= f_0 \partial_z v_g = \frac{g}{T_0}\partial_x T' \quad , \\
\mathcal{L}_{23} = \mathcal{L}_{32} &= -f_0 \partial_z u_g = \frac{g}{T_0}\partial_y T' \quad .
\end{aligned}$$

The matrix $\mathcal{L}$ is symmetric, because the geostrophic wind is divergence-free and because of the thermal wind relation in x and y direction.

The forcing vector $\mathcal{B}$ contains the beta effect, friction, and diabatic heating. It results in

$$\mathcal{B} = \begin{pmatrix} -f_0 \beta u_g - r v_g + D\nabla^2 v_g \\ -f_0 \beta v_g + r u_g - D\nabla^2 u_g \\ \frac{gJ}{c_p T_0} \end{pmatrix} \quad .$$

As the thermal wind relation must be maintained and the geostrophic wind has to stay divergence-free, we also have at the relations

$$-D_g(f_0 \partial_x u_g) = D_g(f_0 \partial_y (v_g)) \quad , \tag{B.47}$$

$$-D_g(f_0 \partial_z u_g) = \frac{g}{T_0} D_g(\partial_y T') \quad \text{and} \tag{B.48}$$

$$D_g(f_0 \partial_z v_g) = \frac{g}{T_0} D_g(\partial_x T') \quad , \tag{B.49}$$

which in conjunction with (B.46) allow to derive diagnostics for $\boldsymbol{\psi}_a$. Calculating the cross-derivatives of the components of (B.46) appearing in (B.47)–(B.49), we can use

the relations (B.47)–(B.49) do derive a diagnostic relation for $\boldsymbol{\psi}_a$.The relations are

$$\begin{aligned}
&\partial_z(\mathcal{L}_{21}u_a)+\partial_z(\mathcal{L}_{22}v_a)+\partial_z(\mathcal{L}_{23}w)-\partial_y(\mathcal{L}_{31}u_a)-\partial_y(\mathcal{L}_{32}v_a)-\partial_y(\mathcal{L}_{33}w)= \\
&\quad=-\partial_z u_g\partial_y(f_0v_g)+\partial_z v_g\partial_y(f_0u_g)+\partial_y u_g\partial_z(f_0v_g)-\partial_y v_g\partial_z(f_0u_g)+\partial_z\mathcal{B}_2-\partial_y\mathcal{B}_3= \\
&\quad=2f_0\frac{\partial(u_g,v_g)}{\partial(y,z)}+\partial_z\mathcal{B}_2-\partial_y\mathcal{B}_3=Q_{yz} \quad , \qquad \text{(B.50)} \\
&\partial_x(\mathcal{L}_{31}u_a)+\partial_x(\mathcal{L}_{32}v_a)+\partial_x(\mathcal{L}_{33}w)-\partial_z(\mathcal{L}_{11}u_a)-\partial_z(\mathcal{L}_{12}v_a)-\partial_z(\mathcal{L}_{13}w)= \\
&\quad=+\partial_z u_g\partial_x(f_0v_g)-\partial_z v_g\partial_x(f_0u_g)-\partial_x u_g\partial_z(f_0v_g)+\partial_x v_g\partial_z(f_0u_g)-\partial_z\mathcal{B}_1+\partial_x\mathcal{B}_3= \\
&\quad=2f_0\frac{\partial(u_g,v_g)}{\partial(z,x)}-\partial_z\mathcal{B}_1+\partial_x\mathcal{B}_3=Q_{zx} \quad \text{and} \qquad \text{(B.51)} \\
&\partial_y(\mathcal{L}_{11}u_a)+\partial_y(\mathcal{L}_{12}v_a)+\partial_y(\mathcal{L}_{13}w)-\partial_x(\mathcal{L}_{21}u_a)-\partial_x(\mathcal{L}_{22}v_a)-\partial_x(\mathcal{L}_{23}w)= \\
&\quad=-\partial_y u_g\partial_x(f_0v_g)+\partial_y v_g\partial_x(f_0u_g)+\partial_x u_g\partial_y(f_0v_g)-\partial_x v_g\partial_y(f_0u_g)+\partial_y\mathcal{B}_1-\partial_x\mathcal{B}_2= \\
&\quad=2f_0\frac{\partial(u_g,v_g)}{\partial(x,y)}+\partial_y\mathcal{B}_1-\partial_x\mathcal{B}_2=Q_{xy} \quad . \qquad \text{(B.52)}
\end{aligned}$$

We can now substitute the ageostrophic wind components with the definition of the ageostrophic stream function to arrive at the combined diagnostic

$$\mathcal{M}(\rho_0\boldsymbol{\psi}_a)=Q=(Q_{yz},Q_{zx},Q_{xy}) \qquad \text{(B.53)}$$

with the entries of $\mathcal{M}$ being

$$\begin{aligned}
\mathcal{M}_{11}&=-\partial_z(\rho_0^{-1}\mathcal{L}_{22}\partial_z)+\partial_z(\rho_0^{-1}\mathcal{L}_{23}\partial_y)+\partial_y(\rho_0^{-1}\mathcal{L}_{32}\partial_z)-\partial_y(\rho_0^{-1}\mathcal{L}_{33}\partial_y) \quad , \\
\mathcal{M}_{12}&=-\partial_x(\rho_0^{-1}\mathcal{L}_{32}\partial_z)+\partial_x(\rho_0^{-1}\mathcal{L}_{33}\partial_y)+\partial_z(\rho_0^{-1}\mathcal{L}_{12}\partial_z)-\partial_z(\rho_0^{-1}\mathcal{L}_{13}\partial_y) \quad , \\
\mathcal{M}_{13}&=-\partial_y(\rho_0^{-1}\mathcal{L}_{12}\partial_z)+\partial_y(\rho_0^{-1}\mathcal{L}_{13}\partial_y)+\partial_x(\rho_0^{-1}\mathcal{L}_{22}\partial_z)-\partial_x(\rho_0^{-1}\mathcal{L}_{23}\partial_y) \quad , \\
\mathcal{M}_{21}&=+\partial_z(\rho_0^{-1}\mathcal{L}_{21}\partial_z)-\partial_z(\rho_0^{-1}\mathcal{L}_{23}\partial_x)-\partial_y(\rho_0^{-1}\mathcal{L}_{31}\partial_z)+\partial_y(\rho_0^{-1}\mathcal{L}_{33}\partial_x) \quad , \\
\mathcal{M}_{22}&=+\partial_x(\rho_0^{-1}\mathcal{L}_{31}\partial_z)-\partial_x(\rho_0^{-1}\mathcal{L}_{33}\partial_x)-\partial_z(\rho_0^{-1}\mathcal{L}_{11}\partial_z)+\partial_z(\rho_0^{-1}\mathcal{L}_{13}\partial_x) \quad , \\
\mathcal{M}_{23}&=+\partial_y(\rho_0^{-1}\mathcal{L}_{11}\partial_z)-\partial_y(\rho_0^{-1}\mathcal{L}_{13}\partial_x)-\partial_x(\rho_0^{-1}\mathcal{L}_{21}\partial_z)+\partial_x(\rho_0^{-1}\mathcal{L}_{23}\partial_x) \quad , \\
\mathcal{M}_{31}&=-\partial_z(\rho_0^{-1}\mathcal{L}_{21}\partial_y)+\partial_z(\rho_0^{-1}\mathcal{L}_{22}\partial_x)+\partial_y(\rho_0^{-1}\mathcal{L}_{31}\partial_y)-\partial_y(\rho_0^{-1}\mathcal{L}_{32}\partial_x) \quad , \\
\mathcal{M}_{32}&=-\partial_x(\rho_0^{-1}\mathcal{L}_{31}\partial_y)+\partial_x(\rho_0^{-1}\mathcal{L}_{32}\partial_x)+\partial_z(\rho_0^{-1}\mathcal{L}_{11}\partial_y)-\partial_z(\rho_0^{-1}\mathcal{L}_{12}\partial_x) \quad , \\
\mathcal{M}_{33}&=-\partial_y(\rho_0^{-1}\mathcal{L}_{11}\partial_y)+\partial_y(\rho_0^{-1}\mathcal{L}_{12}\partial_x)+\partial_x(\rho_0^{-1}\mathcal{L}_{21}\partial_y)-\partial_x(\rho_0^{-1}\mathcal{L}_{22}\partial_x) \quad .
\end{aligned}$$

Equation (B.53) describes three coupled three-dimensional elliptic equations that must be inverted simultaneously. This can be seen as one four-dimensional inversion, in which the fourth dimension comprises the components of $\boldsymbol{\psi}_a$.

Bibliography

Bannon, P. R.: A Model of Rocky Mountain Lee Cyclogenesis, J. Atmos. Sci., 49, 1510–1522, URL http://dx.doi.org/10.1175/1520-0469(1992)049<1510:AMORML>2.0.CO;2, 1992.

Barriopedro, D., García-Herrera, R., Lupo, A. R., and Hernández, E.: A Climatology of Northern Hemisphere Blocking, J. Climate, 19, 1042–1063, URL http://dx.doi.org/10.1175/JCLI3678.1, 2006.

Charney, J. G. and Phillips, N. A.: Numerical Integration of the Quasi-Geostrophic Equations for Barotropic and Simple Baroclinic Flows, J. Meteor., 10, 71–99, doi:10.1175/1520-0469(1953)010<0071:NIOTQG>2.0.CO;2, URL http://dx.doi.org/10.1175/1520-0469(1953)010<0071:NIOTQG>2.0.CO;2, 1953.

Egger, J.: Dynamics of Blocking Highs, J. Atmos. Sci., 35, 1788–1801, doi:10.1175/1520-0469(1978)035<1788:DOBH>2.0.CO;2, URL http://dx.doi.org/10.1175/1520-0469(1978)035<1788:DOBH>2.0.CO;2, 1978.

Egger, J.: Alpine Lee Cyclogenesis: Verification of Theories, J. Atmos. Sci., 45, 2187–2203, URL http://dx.doi.org/10.1175/1520-0469(1988)045<2187:ALCVOT>2.0.CO;2, 1988.

Egger, J.: Interaction of cold-air blocking and upper-level potential vorticity anomalies during lee cyclogenesis, Tellus A, 47, 597–604, doi:10.1034/j.1600-0870.1995.00107.x, URL http://dx.doi.org/10.1034/j.1600-0870.1995.00107.x, 1995.

Egger, J., Spensberger, C., and Spengler, T.: The splitting of synoptic systems at the Rocky Mountains barrier, J. Atmos. Sci., in preparation, 2014.

Junge, M., Blender, R., Fraedrich, K., Gayler, V., Luksch, U., and Lunkeit, F.: A world without Greenland: impacts on the Northern Hemisphere winter circulation in low- and high-resolution models, Climate Dynamics, 24, 297–307, doi:10.1007/s00382-004-0501-2, URL http://dx.doi.org/10.1007/s00382-004-0501-2, 2005.

Keyser, D., Schmidt, B. D., and Duffy, D. G.: A Technique for Representing Three-Dimensional Vertical Circulations in Baroclinic Disturbances, Mon. Wea. Rev., 117, 2463–2494, doi:10.1175/1520-0493(1989)117<2463:ATFRTD>2.0.CO;2, URL http://dx.doi.org/10.1175/1520-0493(1989)117<2463:ATFRTD>2.0.CO;2, 1989.

Langland, R., Tag, P., and Fett, R.: An ice breeze mechanism for boundary-layer jets, 48, 177–195–, URL http://dx.doi.org/10.1007/BF00121789, 1989.

Luo, D.: A Barotropic Envelope Rossby Soliton Model for Block—Eddy Interaction. Part I: Effect of Topography, J. Atmos. Sci., 62, 5–21, doi:10.1175/1186.1, URL http://dx.doi.org/10.1175/1186.1, 2005.

Mc Innes, H., Kristjánsson, J. E., Schyberg, H., and Røsting, B.: An assessment of a Greenland lee cyclone during the Greenland Flow Distortion experiment: An observational approach, Quarterly Journal of the Royal Meteorological Society, 135, 1968–1985, doi:10.1002/qj.524, URL http://dx.doi.org/10.1002/qj.524, 2009.

McCauley, M. P. and Sturman, A. P.: A Study of Orographic Blocking and Barrier Wind Development Upstream of the Southern Alps, New Zealand, Meteorology and Atmospheric Physics, 70, 121–131, doi:10.1007/s007030050029, URL http://dx.doi.org/10.1007/s007030050029, 1999.

Outten, S. D., Renfrew, I. A., and Petersen, G. N.: An easterly tip jet off Cape Farewell, Greenland. II: Simulations and dynamics, Quarterly Journal of the Royal Meteorological Society, 135, 1934–1949, doi:10.1002/qj.531, URL http://dx.doi.org/10.1002/qj.531, 2009.

Papritz, L., Pfahl, S., Sodemann, H., and Wernli, H.: A climatology of cold air outbreaks and their impact on air-sea heat fluxes in the high-latitude South Pacific, J. Climate, accepted., URL http://dx.doi.org/10.1175/JCLI-D-14-00482.1, 2014.

Parish, T. R.: Barrier Winds Along the Sierra Nevada Mountains, J. Appl. Meteor., 21, 925–930, doi:10.1175/1520-0450(1982)021<0925:BWATSN>2.0.CO;2, URL http://dx.doi.org/10.1175/1520-0450(1982)021<0925:BWATSN>2.0.CO;2, 1982.

Pelly, J. L. and Hoskins, B. J.: A New Perspective on Blocking, J. Atmos. Sci., 60, 743–755, doi:10.1175/1520-0469(2003)060<0743:ANPOB>2.0.CO;2, URL http://dx.doi.org/10.1175/1520-0469(2003)060<0743:ANPOB>2.0.CO;2, 2003.

Petersen, G. N., Kristjánsson, J. E., and Ólafsson, H.: Numerical simulations of Greenland's impact on the Northern Hemisphere winter circulation, Tellus A, 56, 102–111, doi:10.1111/j.1600-0870.2004.00047.x, URL http://dx.doi.org/10.1111/j.1600-0870.2004.00047.x, 2004.

Riordan, A. J.: Examination of the Mesoscale Features of the GALE Coastal Front of 24-25 January 1986, Mon. Wea. Rev., 118, 258–282, URL http://dx.doi.org/10.1175/1520-0493(1990)118[258:EOTMFO]2.0.CO;2, 1990.

Schär, C. and Wernli, H.: Structure and evolution of an isolated semi-geostrophic cyclone, Quarterly Journal of the Royal Meteorological Society, 119, 57–90, 1993.

Schwierz, C., Croci-Maspoli, M., and Davies, H. C.: Perspicacious indicators of atmospheric blocking, Geophys. Res. Lett., 31, L06 125–, URL http://dx.doi.org/10.1029/2003GL019341, 2004.

Srock, A. F. and Bosart, L. F.: Heavy Precipitation Associated with Southern Appalachian Cold-Air Damming and Carolina Coastal Frontogenesis in Advance of Weak Landfalling Tropical Storm Marco (1990), Mon. Wea. Rev., 137, 2448–2470, URL http://dx.doi.org/10.1175/2009MWR2819.1, 2009.

Swanson, K. L.: Blocking as a local instability to zonally varying flows, Quarterly Journal of the Royal Meteorological Society, 127, 1341–1355, doi:10.1002/qj.49712757412, URL http://dx.doi.org/10.1002/qj.49712757412, 2001.

Wallace, J. M., Lim, G.-H., and Blackmon, M. L.: Relationship between Cyclone Tracks, Anticyclone Tracks and Baroclinic Waveguides, J. Atmos. Sci., 45, 439–462, URL http://dx.doi.org/10.1175/1520-0469(1988)045<0439:RBCTAT>2.0.CO;2, 1988.

Xu, Q.: Cold and Warm Frontal Circulations in an Idealized Moist Semigeostrophic Baroclinic Wave, J. Atmos. Sci., 47, 2337–2352, doi:10.1175/1520-0469(1990)047<2337:CAWFCI>2.0.CO;2, URL http://dx.doi.org/10.1175/1520-0469(1990)047<2337:CAWFCI>2.0.CO;2, 1990.

Xu, Q. and Keyser, D.: Barotropic and Baroclinic Ageostrophic Winds and Completeness of Solution for the Psi Equations, J. Atmos. Sci., 50, 588–596, URL http://dx.doi.org/10.1175/1520-0469(1993)050<0588:BABAWA>2.0.CO;2, 1993.

Zishka, K. M. and Smith, P. J.: The Climatology of Cyclones and Anticyclones over North America and Surrounding Ocean Environs for January and July, 1950–77, Mon. Wea. Rev., 108, 387–401, URL http://dx.doi.org/10.1175/1520-0493(1980)108<0387:TCOCAA>2.0.CO;2, 1980.